5. ALKALI-METAL CORROSION STUDIES

W. O. Harms R. E. MacPherson

The purpose of this program is to investigate the chemical and metallurgical effects produced in structural materials during exposure to alkali metals. The program is designed to guide the selection of container materials for sodium-cooled fast breeder reactor (LMFBR) systems and lithium-cooled space power reactor systems in which K serves as the Rankine-cycle working fluid. Forced circulation loop experiments of engineering scale are included in the test program.

Mass Transfer of Interstitial Impurities Between Vanadium Alloys and Sodium

J. H. DeVan R. L. Klueh
D. H. Jansen R. L. Wagner

Although vanadium alloys are highly resistant to dissolutive attack by Na, they are quite reactive with nonmetallic impurities in Na, particularly with C, N, and O. Accordingly, we have begun an investigation of the mechanisms by which vanadium alloys are attacked in Na at impurity levels typical of reactor service conditions. Our program is concerned with four basic aspects of the oxidation process for vanadium alloys in Na: (1) the partitioning of O between vanadium alloys and Na; (2) the effects of alloying additions of Cr and Zr on the diffusion coefficient of O in V; (3) the effects of Cr and Zr in V on oxide scale formation and on the dissolution of the alloys in Na; and (4) the solubility of V in Na as affected by the presence of O in either metal. We are also examining the kinetics of carbon and nitrogen transfer between vanadium alloys and types 304 and 321 stainless steel in a sodium circuit.

Oxygen Effects on the Compatibility of Vanadium and Sodium (R. L. Klueh)

We have conducted a series of static capsule tests to evaluate the oxygen partitioning characteristics of pure V and Na and have compared these results with our previous findings for the Nb-Na and Ta-Na systems.

DISCLAIMER

This comparison was of interest because of the much greater solid solubility of O in V than in Ta or Nb.

The experimental system used for these studies consisted of a vanadium specimen in contact with Na in a vanadium container. The capsule, pictured in Fig. 5.1, was made from 0.75-in.-OD × 0.63-in.-ID seamless tubing, and the end caps and specimens were made from 0.060-in.-thick sheet. The results of chemical analysis of the vanadium components are presented in Table 5.1.

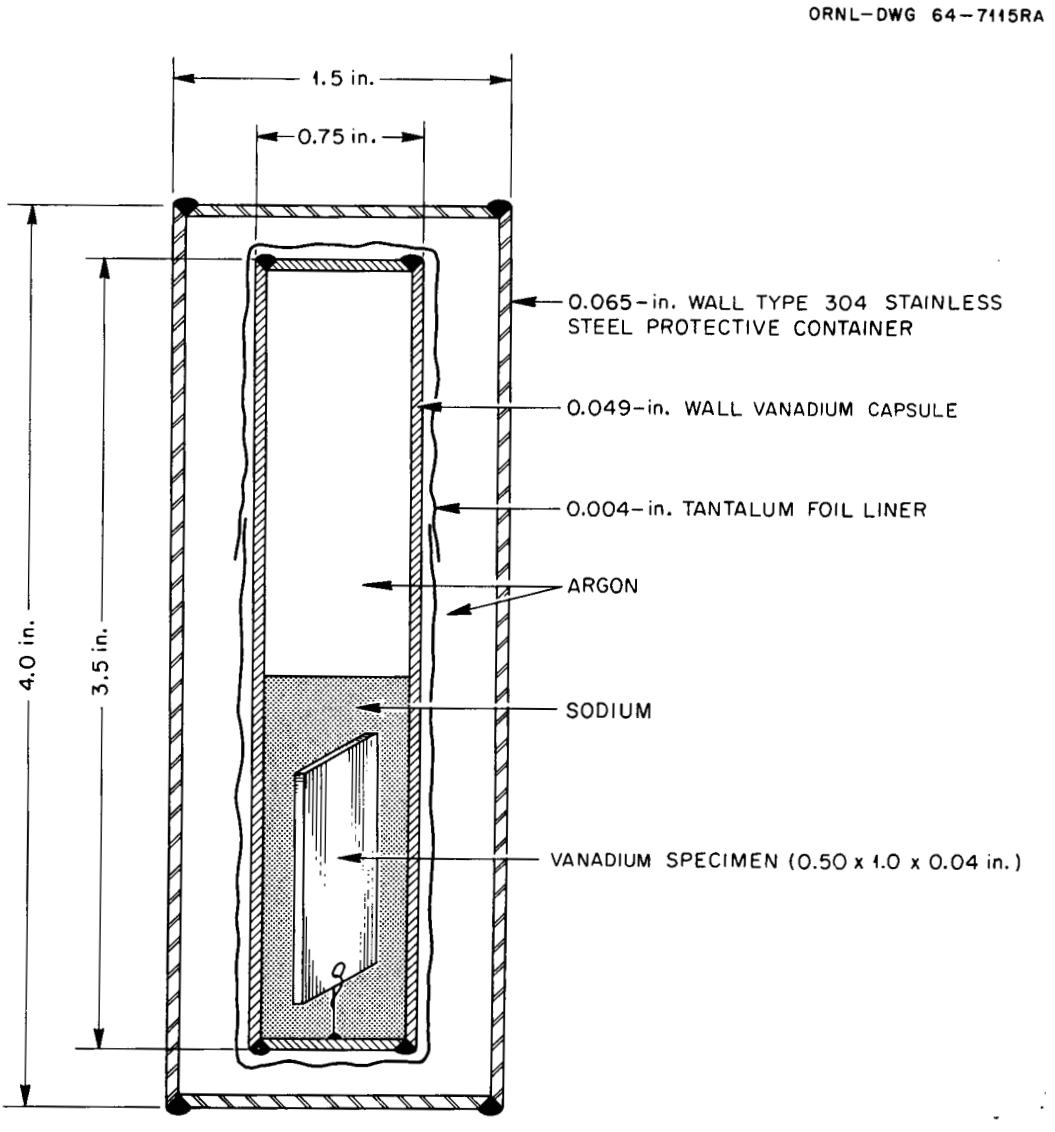

Fig. 5.1. Schematic Drawing of Corrosion Test Capsule Used to Study Oxygen Effects in Vanadium-Sodium Systems.

Table 5.1. Chemical Analysis of Vanadium Components Used in Sodium Compatibility Experiments

Impurity Element	Concentration,[a] ppm	
	Tubing	Sheet
O	1300, 1600	1900
H	2, 10	< 1
N	500, 580	570
C	170, 180	470
Ni	< 10	100
Si	80	80
Ti	40	20
Zr	10	20
Cr	< 4	40
Cu	10	20
Fe	200	500
Mg	20	40
Mn	4	80

[a]Two values indicate duplicate determinations.

The vanadium capsule was protected by an outer container of type 304 stainless steel, and both capsules were sealed under 1 atm of purified Ar. We varied the concentration of O in the Na of the different capsules by adding weighed amounts of Na_2O to the Na and conducted tests at each purity level for 500 hr at 600°C and for 100 hr at 800°C. After testing, each capsule was inverted and quenched in liquid N. The concentration of O in the vanadium specimens and capsules was determined by vacuum fusion analysis; the concentration of O in the Na was calculated by an oxygen mass balance; the vanadium dissolved in Na was analyzed by reacting the Na with isopropyl alcohol and spectrographically determining the concentration of V.

Table 5.2 shows the weight changes and concentrations of O in specimens after exposure to Na. Weight was gained in proportion to the amounts of Na_2O added to the Na before test. A mass balance for O showed that essentially all of the O added had transferred to the

Table 5.2. Weight Changes and Oxygen Analyses of Vanadium Specimens Exposed to Sodium Containing Various Amounts of Na_2O

Temperature (°C)	Initial Oxygen Content of Sodium (ppm)	Specimen Weight Gain[a] (mg)	Final Oxygen Content of Specimen[b] (ppm)
600	50	0.2	1900
	250	0.3	1900
	550	0.4	2100
	850	1.1	2200
	1300	1.6	2300
800	50	0.0	1900
	250	0.0	1900
	550	0.2	1900
	850	0.6	2000
	1250	1.1	2000

[a]Specimen dimensions: 1 × 0.5 × 0.040 in.

[b]Initial oxygen content of vanadium specimen was 1900 ppm.

vanadium specimen and capsule during test. The results differ significantly from those obtained for Nb at 600°C under similar test conditions. As shown elsewhere,[1] Nb containing 70 ppm O acquired O only when the concentration of O in the Na exceeded 1000 ppm, and even then the amount of O transferred was only a small fraction of the total amount present. Thus, the oxygen partitioning coefficient (i.e., $\frac{\text{ppm O in solid metal}}{\text{ppm O in alkali metal}}$) is considerably greater for the V-Na system than for the Nb-Na system.

The amount of V present in the Na after these tests showed little dependence on the amount of O initially added to the Na, but the vanadium concentration did change with test temperature. At 600°C the Na contained only about 40 ppm V, while at 800°C the level was about 200 ppm V. This behavior is in contrast to that of the Nb-Na system,

[1]R. L. Klueh, "Oxygen Effects in the Niobium-Sodium System," pp. 125–126, this report.

in which metal concentrations in the Na increase sharply with additions of O to Na (ref. 1). This further indicates that the O added to Na was rapidly gettered by the vanadium capsule and specimen.

One further distinction between Nb and V concerns the effect of the initial concentration of O in the refractory metal on its attack by Na. At concentrations as high as those initially present in our vanadium samples (1600 to 1900 ppm O), Nb and Ta at 600°C undergo rapid intergranular attack by Na. Vanadium samples in these tests, however, showed no evidence of attack by Na. We believe this difference in behavior reflects the difference in the solid solubility of O in the two materials. At 600°C, 1900 ppm O in Nb is above the solubility limit, whereas this level is only about 20% of the solubility limit of V.

Interstitial Mass Transport Between Type 300 Series Stainless Steels and Vanadium Alloys (J. H. DeVan, D. H. Jansen)

Shown in Fig. 5.2 is the design we have adopted for a thermal convection loop to evaluate the transport rates of N and C between vanadium alloys and stainless steels in a sodium circuit. Heated portions of the loops are being constructed of V or its alloys, and the isothermal and cooled portions are of either type 304 or 321 stainless steel. Brazed bimetallic joints are used to couple the dissimilar loop sections. Figure 5.3 shows the joint design, which is patterned after that used for earlier Nb–1% Zr–stainless steel bimetallic loop studies. Several joints fabricated by this technique have been examined metallographically, one after four thermal cycles between room temperature and 800°C. All of the joints appeared sound, and all passed a leak check with a helium mass spectrometer.

Mass transfer rates and interstitial effects on mechanical properties will be monitored in these loop systems by means of insert specimens placed in both the heated and cooled sections of the loop. The inserts, shown in Fig. 5.4, are small, round tensile specimens (1/8-in.-diam gage section) that are joined end-to-end to form a continuous, concentrically positioned rod running the entire length of each vertical loop section.

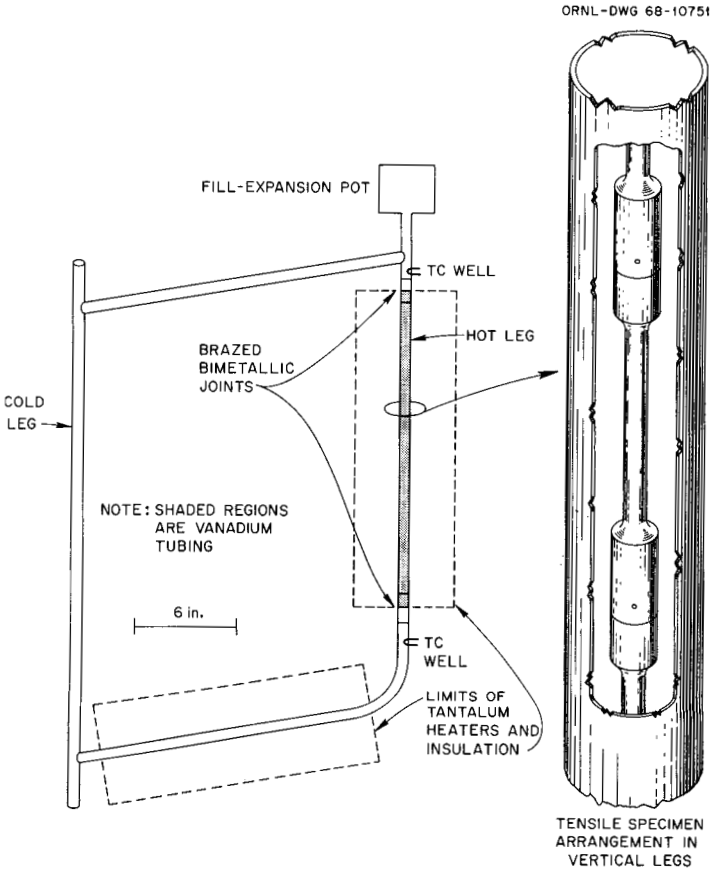

Fig. 5.2. Bimetallic Thermal Convection Loop Designed to Study Interstitial Mass Transport Between Vanadium Alloys and Sodium.

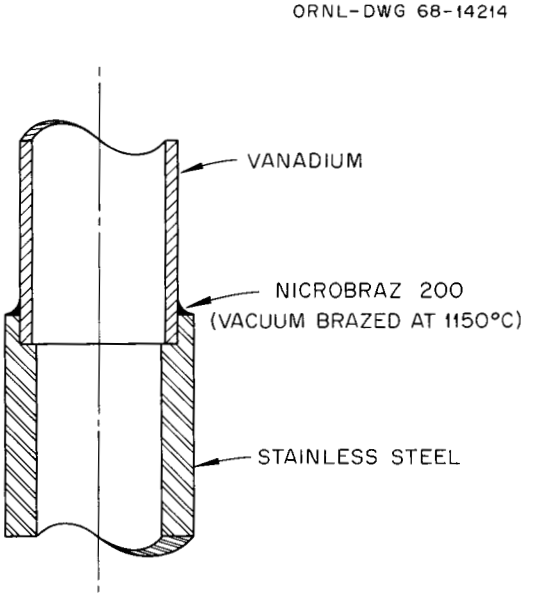

Fig. 5.3. Braze Joint Design for Vanadium-Stainless Steel Thermal Convection Loop System.

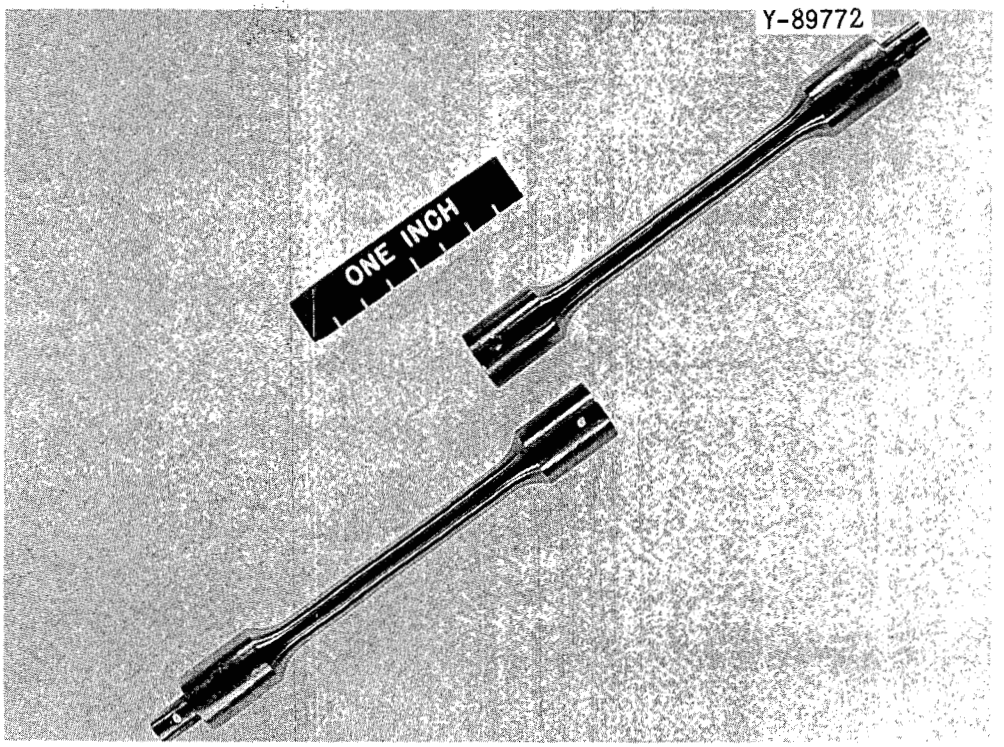

Fig. 5.4. Insert Specimen Designed for Bimetallic Thermal Convection Loop Studies.

We have completed the fabrication of three loops with hot-leg sections of pure V and cold-leg sections of type 304 stainless steel. Two similar loops with type 321 stainless steel cold legs are also being constructed. Operation of these loops is awaiting the fabrication at ORNL of developmental V-Cr alloys and the delivery of Westinghouse Vanstar alloys. Both types of materials will be used as insert specimens.

Interstitial Effects on Mechanical Properties of Vanadium Alloys
(R. L. Wagner)

As discussed above, the pickup of interstitial impurities from Na is a critical consideration in the development and use of vanadium alloys for LMFBR cladding. Of special concern are the effects this contamination may have on creep properties and the ductile-to-brittle transition temperature of candidate alloys. For this reason, mechanical properties rank very high in the list of effects to be evaluated in our analysis of corrosion specimens. To supplement this effort, we are also

planning investigations of the mechanical properties of specimens to which contaminants have been added from a low-pressure ($< 10^{-9}$ torr) gas. This possibility was suggested in conjunction with absorption studies that are under way to provide oxygen-doped vanadium samples for corrosion testing. We plan to correlate the creep properties of alloys contaminated with single impurities from a gaseous atmosphere with the effects on creep brought about by corrosion exposures.

Data recently published by Hörz[2] show that above 900°C engassing kinetics for pure V in rarified O_2 are controlled by the rate at which O_2 arrives at the vanadium surface and that the reaction rate is therefore directly proportional to pressure. We are extending these findings to temperatures of interest for our creep studies, 500 to 900°C.

Compatibility of Stainless Steel and Insulation in LMFBR Systems

A. P. Litman

This new task is a two-year effort designed to guide the selection of containment piping and thermal insulation for LMFBR systems and is in direct support of the Fast Flux Test Facility (FFTF). The structural materials for the FFTF closed sodium loops, while not yet fixed, will probably be types 304, 316, or 321 stainless steel operating at 370 to 760°C. A question not yet factored into the criteria for selection of materials for these loops is the extent to which the long-term oxidation resistance of these stainless steels will be affected by interaction with thermal insulating materials or a sodium leak. This task includes a comprehensive study of the literature and tests of the compatibility of stainless steels and thermal insulation in air and inert gas, with and without the presence of Na.

---

[2]G. Hörz, Z. Metallk. 59, 180 (1968).

Effect of Insulation on Oxidation of Stainless Steel (C. D. Bopp)

Years of experience have led to reliable insulation practices for dynamic sodium systems constructed of stainless steels; but most of this is highly empirical, and information is lacking in the areas of long-term, cyclic, and transient effects.

Table 5.3 shows some of the typical insulation materials used at ORNL and their chemical compositions, basically silica and alumina. The insulations are generally manufactured by jet blasting a molten mixture of minerals to produce relatively short ceramic fibers. Spinning produces longer fibers. By combining different lengths of fibers with or without a binder by various techniques, manufacturers can produce papers, blankets, felts, ropes, braids, boards, blocks, textiles, tubes, and cast shapes. In addition to the materials detailed in Table 5.3, a wide variety of more expensive insulations are available, suitable for LMFBR service to 760°C. These include almost pure oxides [i.e., SiO_2 (Glasrock, Min-K 1301, Refrasil, Astroquartz)], porous Al_2O_3, and porous ZrO_2.

Oxidation and Catastrophic Oxidation of Stainless Steel. — The resistance of stainless steels to mildly oxidizing conditions is well known and is attributed to the protective nature of chromium-rich oxides that form on the surface of the metal. Experience and examination of available thermodynamic data indicate that in the temperature range of interest, to 760°C, no reaction should occur between the oxides of Fe, Cr, or Ni on stainless steel and pure alumina or silica. However, the presence of low-melting and volatile oxides, S, and the halogens, combined or in elemental form, can lead to catastrophic oxidation at the interface between base metal and oxide. One of the possible causes is believed to be the formation of liquid or semiliquid phases that destroy the protective oxides. The result is the onset of extremely rapid corrosion accompanied by the formation of voluminous corrosion products. Numerous studies have demonstrated that oxidation occurs at normal, often parabolic, rates up to the melting point of binary or ternary eutectic mixtures (including the foreign substance). Above these definite temperatures, oxidation occurs at a linear or accelerating

Table 5.3. Typical Thermal Insulating Materials Presently Used for Stainless Steels

Aluminum Silicate Fibers Trade Name	Calcined Diatomaceous Silica Trade Name	Nominal Analysis, wt %							
		Al_2O_3	SiO_2	Fe_2O_3	B_2O_3	TiO_2	Na_2O	CaO	MgO
Fiberfrax[a]		51	47		0.6				
Kaowool[b]		45	51	1	0.1	2	0.2	0.1	Trace
Thermoflex[c,d]		42	50			6			
	Superex[c]	6	81	5		0.1		1	6

[a]Total Fe_2O_3, CaO, and MgO = 0.5 wt %. Manufactured by Carborundum Company.

[b]Manufactured by Babcock & Wilcox Company.

[c]A Johns-Manville Company product.

[d]Total other impurities which probably consist of Fe_2O_3, B_2O_3, Na_2O, CaO and MgO = 2 wt %. The analysis does not include a small amount of organic binder.

rate and is catastrophic. There are several other mechanisms by which oxidation may be accelerated by impurities. A common one is an increase in the semiconductivity of the oxide film, which may enhance reactions at the interface of oxide and gas.[3] Another possibility is an increase in the number of cation vacancies, although it has been shown that a number of thermodynamic variables must be considered in this case.[4] Though several postulates have been proposed to explain the actual details of the corrosion mechanism(s), much disagreement still exists. This is not surprising, since even the normal oxidation behavior of stainless steels still has not been described by a unified mechanism.

Numerous examples of catastrophic oxidation have been reported, including the corrosion of boiler tubes because of the presence of V or Na in low-grade fuels and Na or S in the atmosphere. Water vapor in the air has been found to aggravate this type of corrosion.[5] Furnace manufacturers have long been plagued with extensive corrosion of heater elements due to the presence of impurities such as PbO, MoO_3, WO_3, V_2O_5, Na_2O, Na_2SO_4, and NaCl in the furnace insulation. At ORNL, certain types of Sauereisen cements containing Na_2SiO_3 have produced catastrophic oxidation of type 316 stainless steel at 760°C (Fig. 5.5).

Oxidation resistant alloys that are particularly susceptible to catastrophic oxidation include types 316 and 317 stainless steel, 19-9 DL, N-155, Refractaloy B, and 16-25-6 alloy. All of these alloys contain Mo, and the 19-9 DL and N-155 alloys also contain 1 to 2% W. Both Mo and W form highly volatile, mobile oxides. It is believed that the molybdenum oxide vapors that evolve on heating accumulate in stagnant atmospheres cause catastrophic attack.

Experimental Approach. — Because of the short time allowed for this portion of the program, our experimental approach for determining the effect of insulation on the oxidation of stainless steel is reduced to an investigation of whether various commercial thermal insulations will

---

[3]J. H. Eriken and K. Hauffe, Z. Physik. Chem. 59, 332 (1968).

[4]K. Hauffe, Oxidation of Metals, p. 304, Plenum Press, New York, 1965.

[5]H. L. Logan, Corrosion 17, 185t (1961).

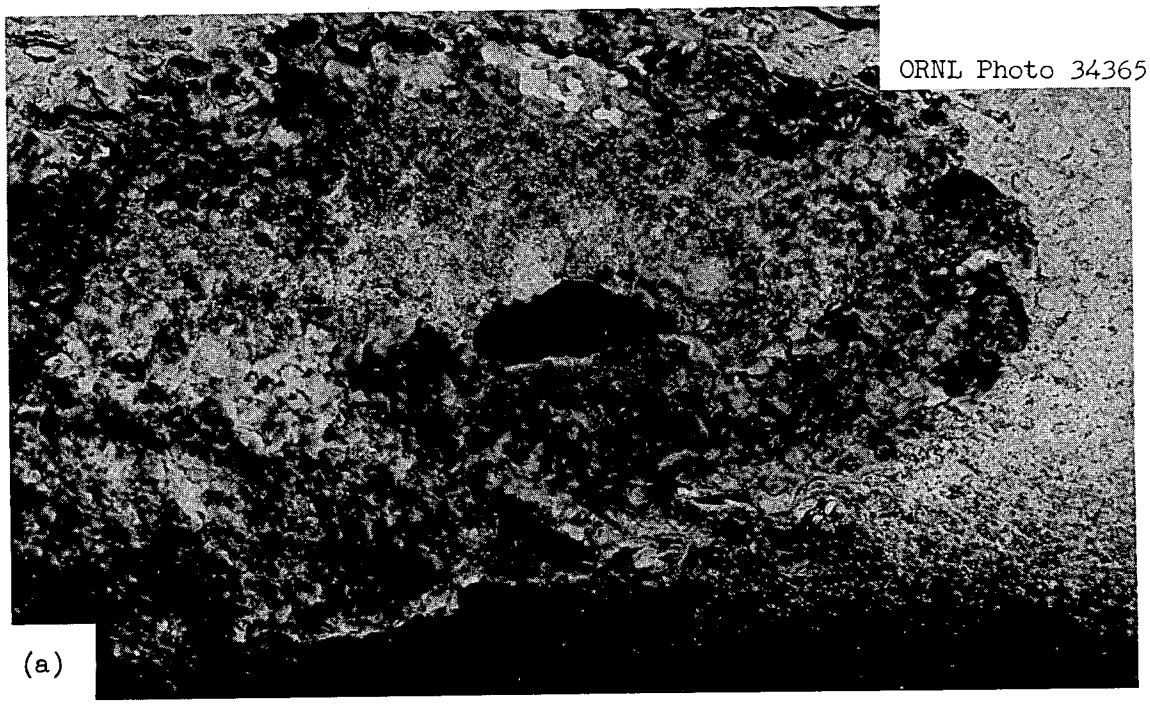

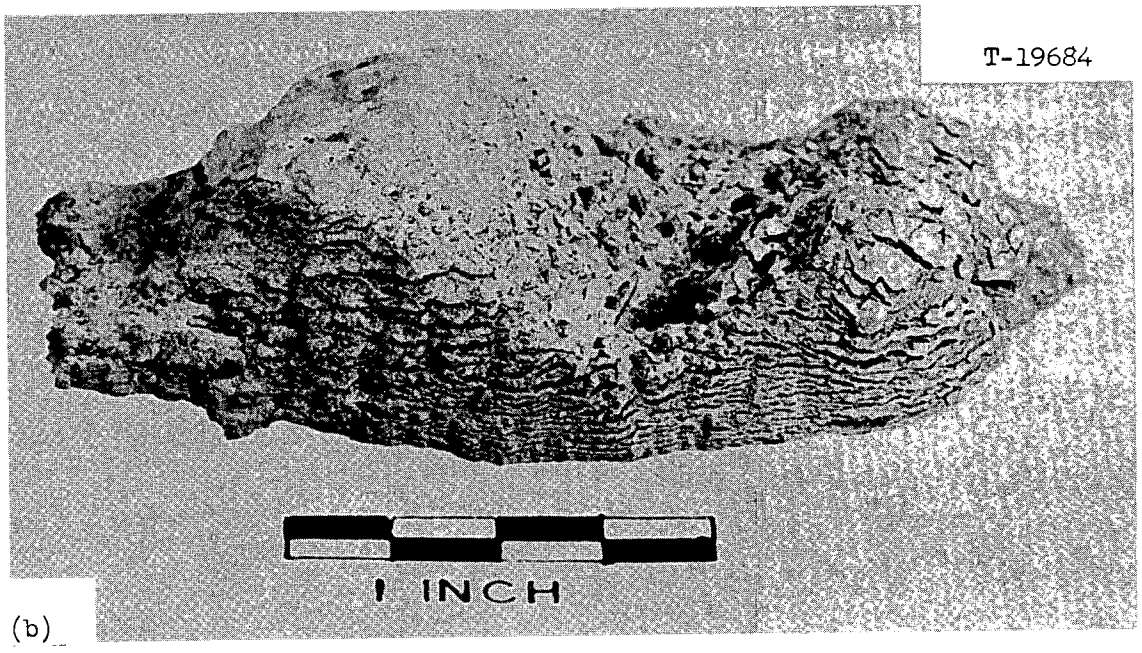

Fig. 5.5. Area of Catastrophic Oxidation Induced by Contact with Sodium Silicate that Produced Failure of Type 316 Stainless Steel 2-in. Sched-40 Pipe at 760°C. (a) Zone of failure after removal of oxide products; (b) oxide products.

induce catastrophic oxidation. If we find this, we will identify the impurity responsible. If the condition is only active during local atmosphere stagnation, we will characterize the system to determine preventative conditions.

A schematic of our experimental setup — almost complete at the time of this writing — is shown in Fig. 5.6. Specimens (coupons or tubes)

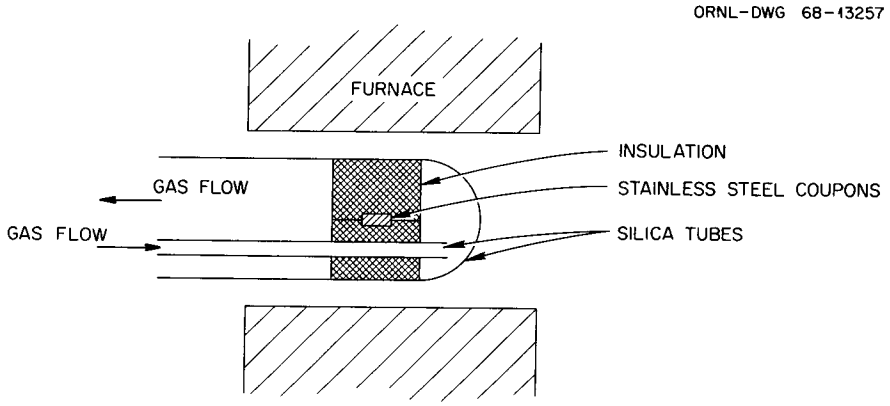

Fig. 5.6. Experimental Arrangement for Determining Compatibility of Stainless Steel with Thermal Insulation.

will be packed in insulation and oxidized isothermally in air or other atmosphere with a given moisture content. In some instances, the permeability of the insulation will be controlled by compressing it to various extents, and air will be forced to flow through the insulation at a given rate. In other tests, the space between the insulation and the specimens will be varied. The amount of oxidation will be determined by oxygen consumption, weight change after descaling, standard metallographic techniques, electron microprobe traces, and/or other means as necessary.

The effect of surface condition — often important in oxidation studies — will be investigated by pretreatment of the specimens. It is already known that work hardening affects the chromium content (and therefore the protective nature) of the scale that initially forms when stainless steels are heated. We will study the effect of moisture by regulating the moisture content of the gas, and in most cases we will remove moisture from the insulation with circulating dry air at about

300°C before test. Thermal cycling will be used to test the resistance of the surface scale to spalling. In some experiments, we will study the effect of stress by the use of C-ring specimens fabricated from tubing.

Effect of Sodium on Oxidation of Stainless Steel – Insulation Couples (C. D. Bopp)

Because leaks are always possible in closed sodium systems, we intend to record and categorize the events that take place during a sodium leak in stainless steel containment lagged with insulation. It is well known that the presence of sodium liquid or vapor greatly aggravates the oxidation of high-temperature alloys. As previously discussed, the fluxing of previously formed protective scales is a particularly destructive mode of attack. In this respect, the mixtures with relatively low melting points (shown below) that may form by interaction of Na, O, aluminum silicate insulation, and metal in LMFBR systems are important:

Components	Melting Temperature, °C
Na_2O-Fe_2O_3-SiO_2	800
Na_2O-Fe_2O_3-Al_2O_3-SiO_2	715, 728
Na_2O-FeO-SiO_2	667
Na_2O-FeO-Al_2O_3-SiO_2	< 667
Na_2O-MoO_3	510

For simplicity, we have omitted consideration of Na_2O_2 and NaOH, although these compounds could also form under the proper conditions. The Na_2O_2 is most likely to be present at lower temperatures (< 550°C), and some NaOH will be formed in moist gases. The presence of these additional components may lower the melting points substantially below the values listed above.

Small Leaks. – In the lower range of temperatures for LMFBR systems, a small leak may be self-sealing. (This possibility would be a function of the absorbency of the insulation.) In such cases the attack on stainless steel would be minimized. At these lower temperatures, a small leak – even if it were not sealed by Na soaking into the insulation – would probably be less destructive, be more localized, and require less

extensive repair to the affected areas. In any event, corrosion will be minimized if the leak is detected at the earliest possible moment and the affected insulation is replaced.

We will examine the problem of small leaks with the test device shown in Fig. 5.7. The leak is simulated by unplugging a small hole in a stainless steel capsule containing Na. After a given time, the amount of corrosion of the capsule is determined. Leakage will be studied in Ar as well as in air, since the data for Ar will be applicable to installations where an inert cover gas is used. It is possible that in Ar the Na may react with the insulation to produce products that corrode stainless steel, although in air it is likely that most of the corrosion will be produced by Na_2O and Na_2O_2.

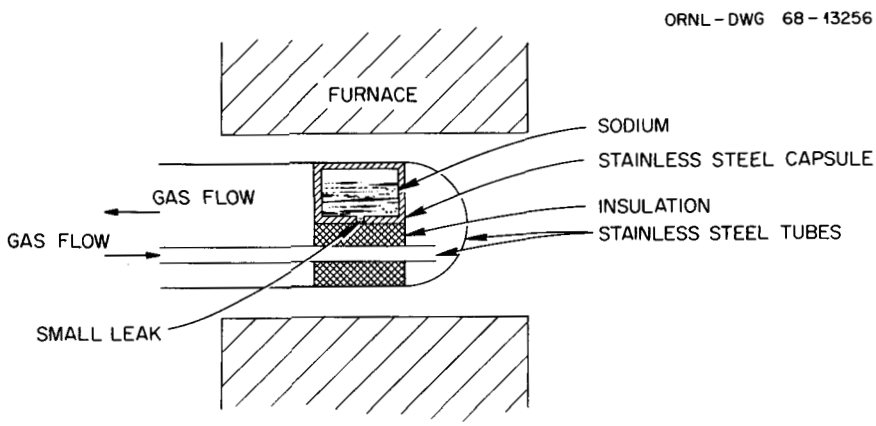

Fig. 5.7. Experimental Setup for Evaluating the Effects of Small Sodium Leaks in Stainless Steel–Thermal Insulation Systems.

Large Leaks. – It is probable at higher temperatures in LMFBRs that any leak will soon become a large leak. In order to test this and the influence of various insulations in proximity to the leak, we are constructing the test device shown in Fig. 5.8. In order to simulate as closely as possible LMFBR and FFTF conditions, we will heat the test pot with an immersion heater. This will induce temperature gradients similar to LMFBR conditions. The sodium pressure against the leak (and the sodium flow) will be maintained by inert gas pressure.

Leak Detection. – Early detection of leaks is important in LMFBR systems, and continuous sampling of the air confined by the insulation

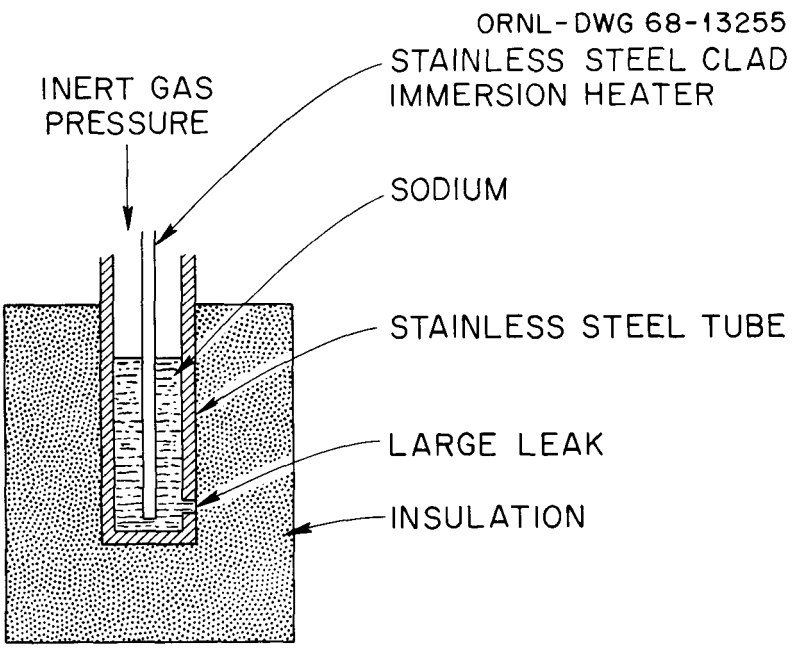

Fig. 5.8. Schematic of Pot Test for Determining Effect of a Large Sodium Leak in Stainless Steel Containment Lagged with Thermal Insulation.

may accomplish this. There are several possibilities for the sensing device for such a system, but perhaps a standard coulometric instrument[6] sensitive to oxidizing vapors will prove satisfactory. We will investigate the sensitivity of this method by using it to monitor the Na_2O aerosol produced in some of the experiments already described.

Corrosion of Refractory Alloys in Lithium, Potassium, and Sodium

J. H. DeVan A. P. Litman W. R. Huntley

Auxiliary electrical or ion-propulsion requirements for space vehicles necessitate power plants of high efficiency that will operate at high temperatures. For these applications, nuclear power systems have been proposed in which alkali metals are used to transfer heat, drive a turbogenerator, and lubricate rotating components. Accordingly, we are investigating the corrosion properties of candidate alkali metals,

[6]R. L. Chapman, Instr. Control Systems 41, 79 (1968).

primarily Li and K, under conditions of interest for space applications. Because of the relatively high temperatures (> 1000°C), the investigation is concerned largely with refractory metal container materials.

Compatibility of Boiling Potassium with Refractory Alloys

Refluxing Capsule Experiments (J. R. DiStefano). — We have reached a logical termination point in our study of the effects of refluxing K on refractory metals. Accordingly, although two tests in operation will be continued to 5000 hr, we plan no additional tests. A topical report has been written[7] covering all but the most recent tests, some of which are discussed below.

We have examined two W–26% Re refluxing capsules which, as reported last quarter,[8] operated for 5000 hr at a boiler-condenser temperature of 1250°C. The two capsules were of similar dimensions (0.86 in. outside diameter × 0.040 in. wall thickness × 12 in. long), but one was fabricated from a powder metallurgy product and the other from an arc-melted ingot. Both were tested in the as-extruded condition.

Our examination of the powder-product capsule showed no measurable corrosion effects in either the condenser or boiler sections. However, the capsule fabricated from arc-melted material, as shown in Fig. 5.9, contained a ring of crystalline deposit in the condenser section about 1/2 in. below the top end cap. Figure 5.10 shows the metallographic appearance of the wall of this capsule at several positions along its length. The deposit is clearly visible in the upper-left photomicrograph and is seen to be integral with the condenser wall. The boiler wall has undergone subsurface attack, the depth increasing with distance down the boiler. An electron-probe microanalysis of the deposit showed it to consist of almost pure W. Results of the microprobe scan are shown

---

[7] J. R. DiStefano, Refluxing Capsule Experiments with Refractory Metals and Boiling Alkali Metals, ORNL-4323, in preparation.

[8] J. R. DiStefano, Fuels and Materials Development Program Quart. Progr. Rept. June 30, 1968, ORNL-4330, p. 82.

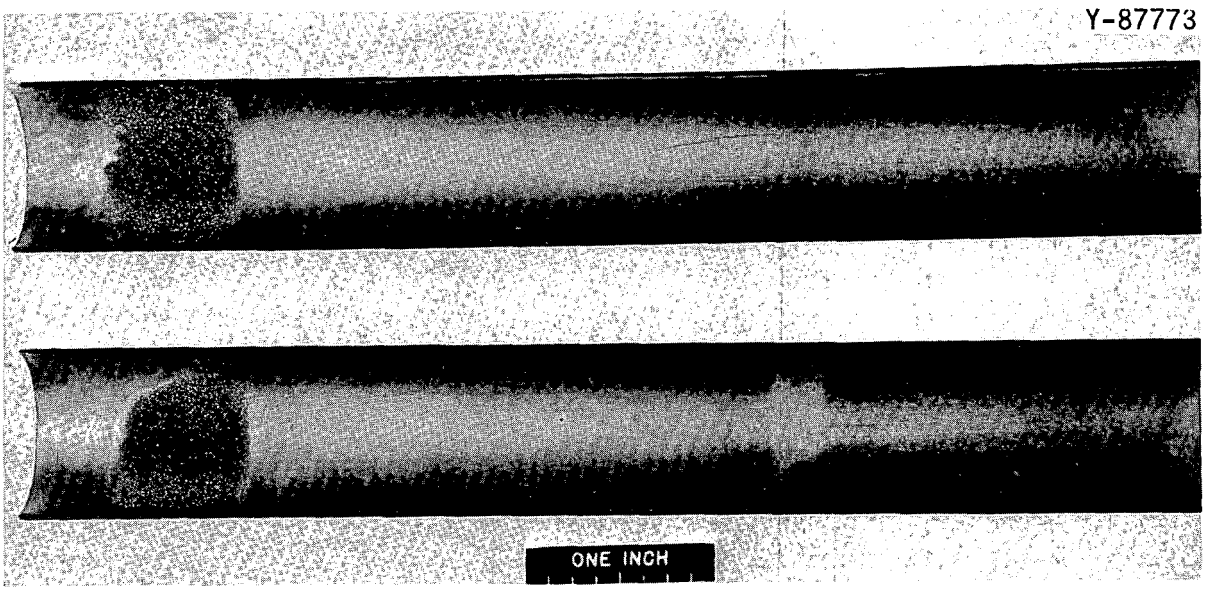

Fig. 5.9. Tungsten Mass Transfer Deposit in Condenser Section of Arc-Melted W–26% Re Capsule Containing Boiling Potassium for 5000 hr at 1250°C.

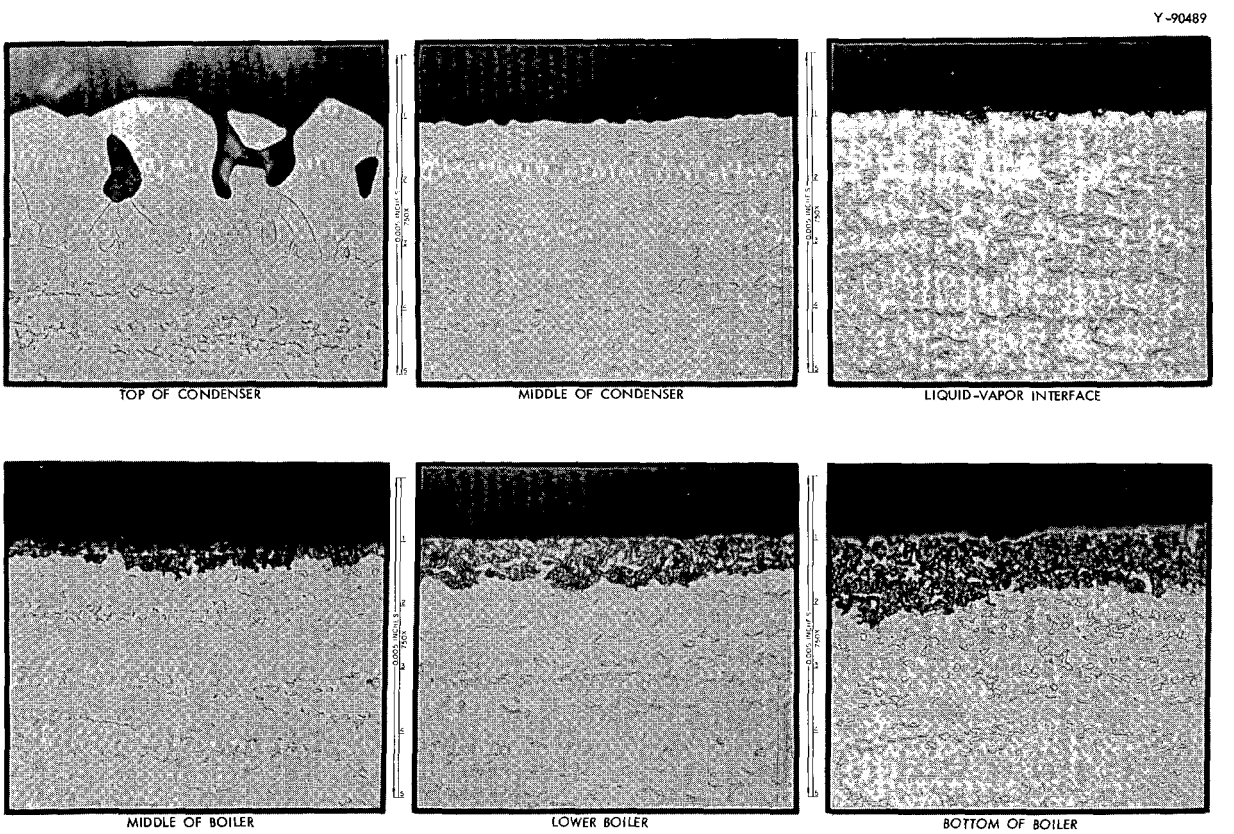

Fig. 5.10. Metallographic Appearance of W–26% Re Refluxing Capsule that Operated with Boiling Potassium for 5000 hr at 1250°C. (Capsule was made from an arc-cast extrusion.)

in Fig. 5.11. This result correlated with analysis of the boiler wall, which, as shown in Fig. 5.12, was depleted of W and enriched in Re in the attack zone.

In speculating as to the cause of the preferential tungsten mass transfer in this capsule, we must account not only for the inverse nature of the deposition (i.e., in the condenser rather than the boiler), but also for its occurrence in only one of the two W–26% Re capsules tested. We believe that none of the classical solution-deposition modes put forth for refluxing potassium systems is compatible with our observations and that some other mechanism must be operating. Results observed in our pure niobium capsules, reported last time,[9] may give a clue to this other mechanism. We noted in the case of pure Nb that, as a consequence of depletion of O from the condenser regions, we acquired a small amount of O in the K in the boiler region. Based on Nb-K static capsule tests, the level of O in the K was still far below that which should have led to migration of O into the Nb or to serious oxidative corrosion. Nevertheless, we have observed both effects in refluxing systems. This strongly suggests that, because of the boiling process, the activity of O at the boiler surface locally exceeds that associated with the "mixed-mean" concentration of O. Such an effect could also explain the deposits of W at the top of the capsule. Free energy considerations suggest that, at 1200°C, the oxygen activity needed to form WO_2 is considerably below the activity reached in a saturated solution of O in K. If the local oxygen activity were sufficient to form WO_2, it is not unreasonable, in view of the relatively high vapor pressure of this oxide, that WO_2 molecules could be swept along with potassium vapor to the condenser.[10] Once outside the region of locally high oxygen activity, any WO_2 molecules would encounter strongly reducing conditions. So long as they

---

[9] J. R. DiStefano, Fuels and Materials Development Program Quart. Progr. Rept. June 30, 1968, ORNL-4330, pp. 75–84.

[10] A similar conclusion could be drawn for thermally stable compounds of the type $K_x W_y O_z$. [See H. Kessler, A. Hatterer, and A. Herald, "Action of Alkali Metal Vapours on the Trioxides of Molybdenum and Tungsten," pp. 465–473 in The Alkali Metals, Chem. Soc. (London) Spec. Publ. 22. The Chemical Society, London, 1967.]

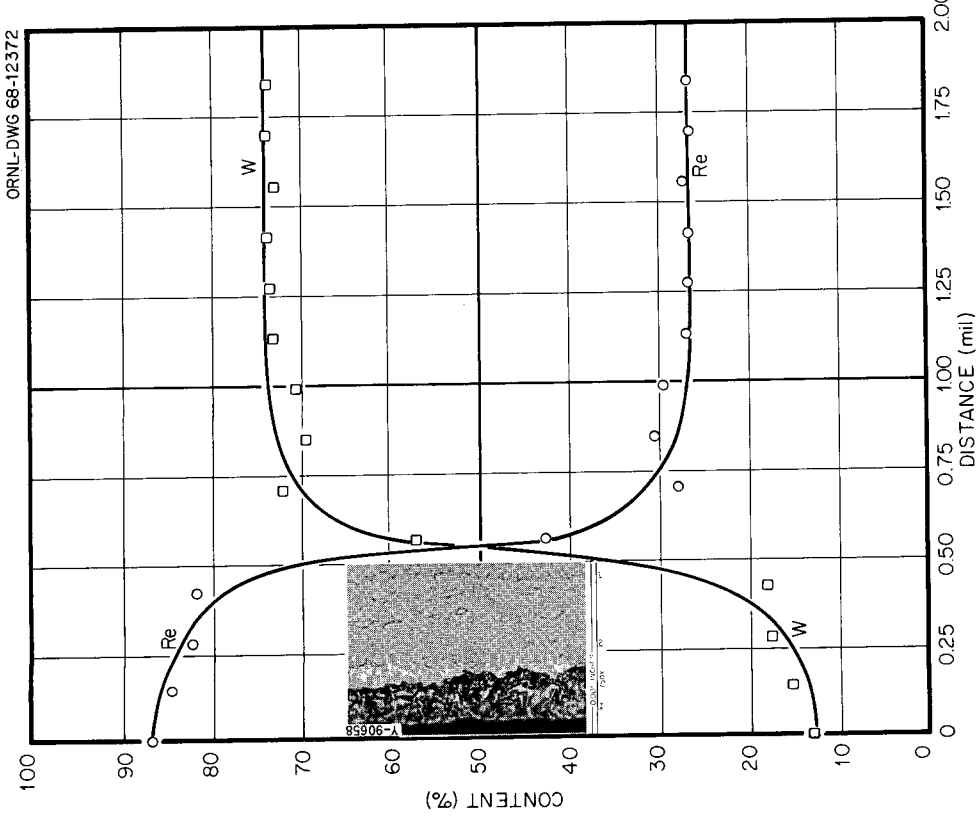

Fig. 5.12. Electron-Probe Scan of Boiler Region of W–26% Re Capsule After 5000 hr in Potassium at 1250°C.

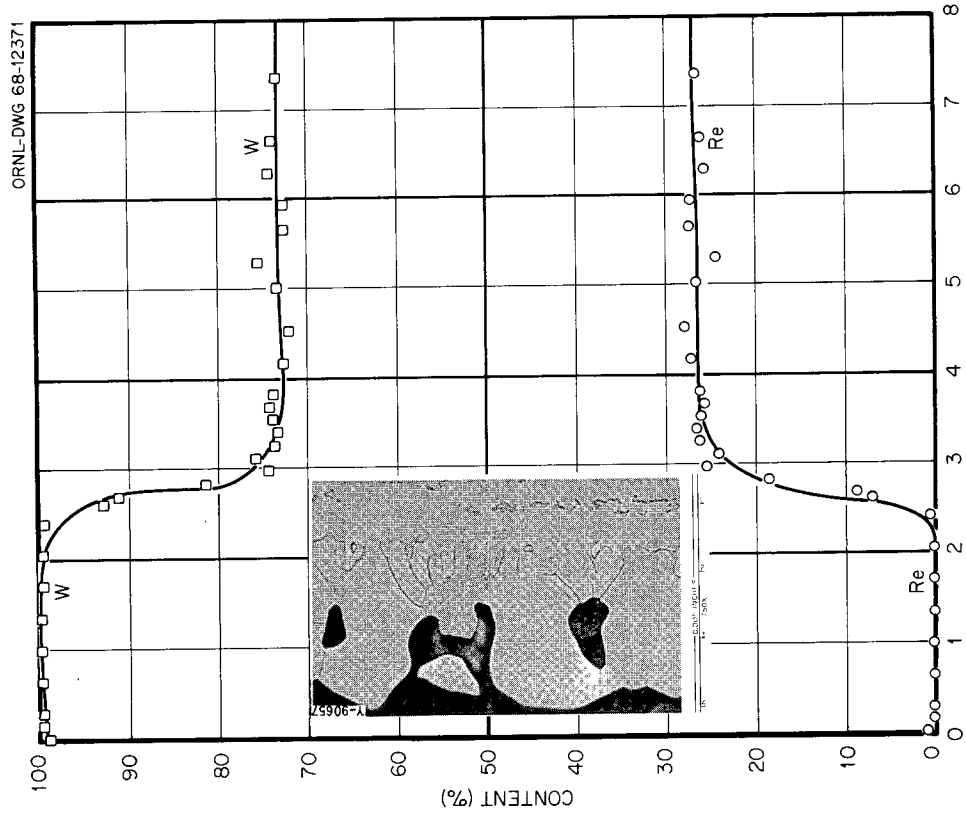

Fig. 5.11. Electron-Probe Scan of Condenser Section of W–26% Re Capsule After 5000 hr in Potassium at 1250°C.

were surrounded by vapor, however, reaction would be dependent on collisions in the gas state, a process sufficiently slow that some of the WO_2 molecules (acting as a noncondensible) could conceivably reach the top of the capsule. Here they would remain trapped until reduction occurred, probably as a heterogeneous reaction at the capsule wall. Oxygen would then be recycled via the condensate back to the boiler region.

Whatever the reasonableness of the above speculation, there is evidence to support the belief that O contributed to the observed mass transfer. This is based on the fact that the arc-melted W–26% Re capsule in which mass transfer was found originally contained about three times more O (about 60 ppm) than the deposit-free capsule (about 20 ppm O). As a consequence of this, the level in the boiler wall in the former capsule increased to almost 140 ppm O, while that in the latter capsule did not increase measurably above the starting level of about 20 ppm O. Neither test showed any measurable amount of W or Re in the K after operation.

Natural Circulation Boiling Potassium Loops (D. H. Jansen). — As reported last quarter,[11] we have concluded a series of natural circulation boiling loop experiments designed to evaluate the effects of boiling K on refractory metals. The final loop in this series was constructed of the molybdenum-base alloy TZM and was operated under the following test conditions.

Boiler-condenser temperature	1200°C
Subcooler temperature	650°C
Condensing rate	R total = 42 g/min
	$\frac{dR}{dA} = (0.13\ g\ min^{-1}\ cm^{-2})$

The loop completed 4400 hr of a scheduled 5000-hr test run and was stopped by a creep failure in the vapor line.

The condition of the loop after operation is shown in Fig. 5.13. Only the upper left-hand corner of the loop, where the failure occurred,

[11] D. H. Jansen, Fuels and Materials Development Program Quart. Progr. Rept. June 30, 1968, ORNL-4330, pp. 84–85.

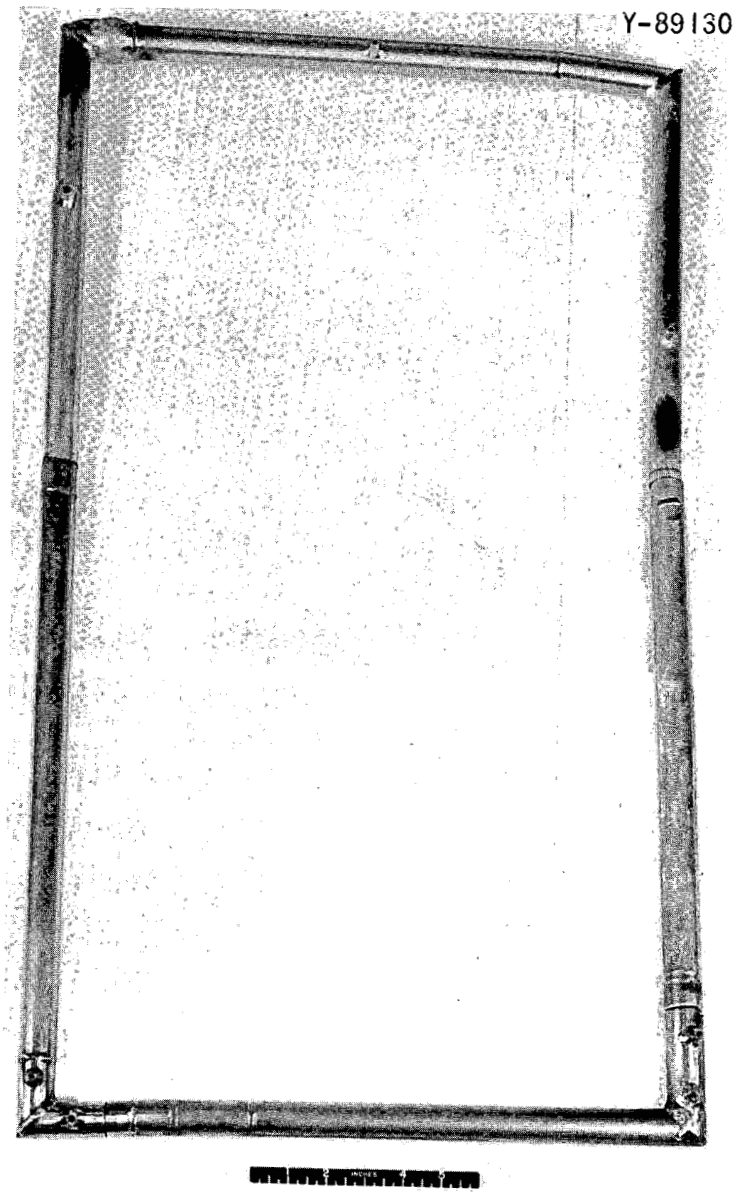

Fig. 5.13. Alloy TZM–Boiling Potassium Loop Showing Configuration of Mitered Corners. Rupture is at upper left-hand corner.

showed any change in macroscopic appearance. As shown at a higher magnification in Fig. 5.14, the failure occurred in a short section of tubing that joined the horizontal dryer section to the vertical condenser leg. This short tubing section was part of an original dryer segment that had to be replaced after 1300 hr of operation because of a similar creep failure under the dryer heater upstream of the later failure. The short section was left in place because (1) it was located well away from the

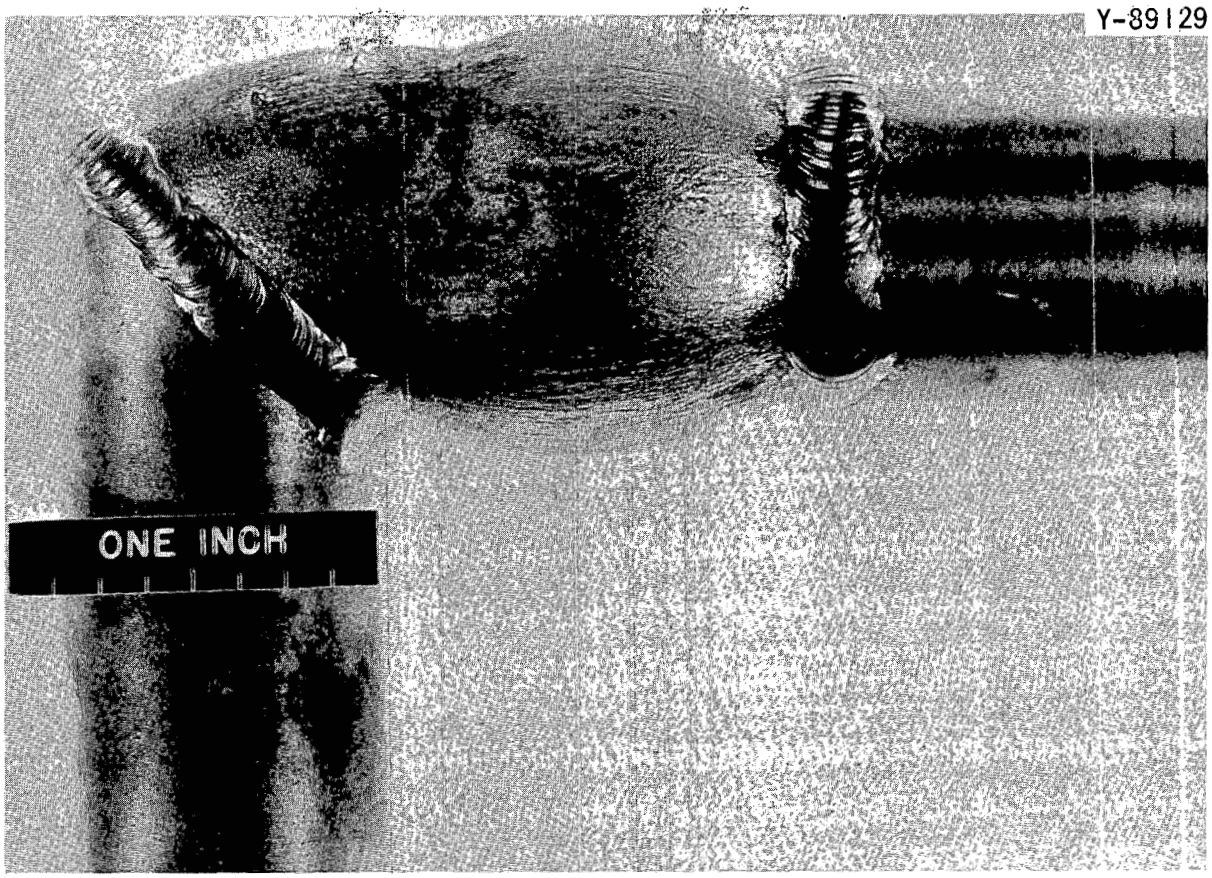

Fig. 5.14. Failure Area of TZM Loop Showing Deformation of Tubing Comprising the Vapor Carryover Line. Vertical leg is top of condenser area.

dryer heater, (2) it had shown no deformation in 1300 hr, and (3) the new dryer section was more easily attached by not running it all the way to the miter joint (Fig. 5.14). However, this short section of the original dryer did constitute a weak link, since it had less wall thickness than either the new dryer line or the adjoining condenser leg. Although long-term creep data on TZM are limited, the available data suggest that the failure of this section can be explained by time-temperature-stress conditions without recourse to a weakening effect of the K.

Weight changes of insert specimens contained in the condenser and subcooler sections of this loop were discussed last quarter.[11] Specimens from the condenser showed little weight change, while subcooler specimens gained an average of 10 mg/cm^2. The metallographic appearance of representative inserts from these respective loop sections is compared in Fig. 5.15. Note that recrystallization took place in both regions with

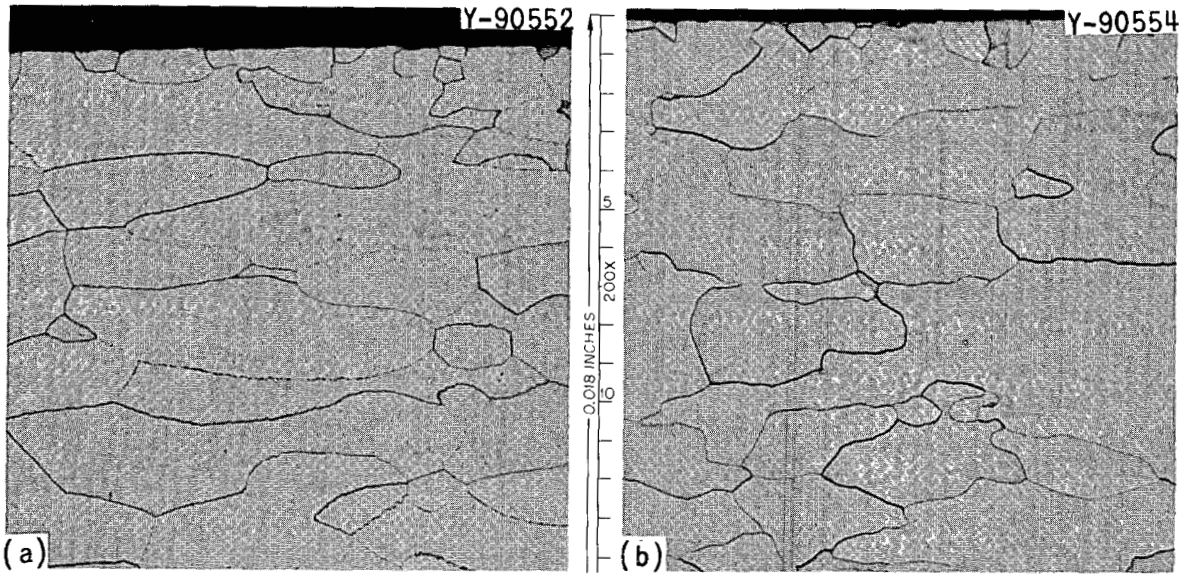

Fig. 5.15. Views Showing Inside Surface of (a) Boiler at Approximate Liquid-Vapor Interface, About 1250°C, and (b) Horizontal Vapor Line, About 1200°C. The material in (b) was from a more recent and purer heat. Etchant: H_2O-H_2O_2-H_2SO_4.

the exception of a narrow zone bordering the exposed surface. We are examining this region to determine what chemical changes may have occurred to cause the apparent grain stabilization.

Specimens from the boiler and dryer regions showed no changes from before-test specimens other than recrystallization and grain growth (Fig. 5.16). Specimen temperatures in the lower subcooler region were apparently below the recrystallization threshold, and these specimens were entirely similar in appearance to before-test specimens.

Forced Circulation Boiling Potassium Loop Tests (FCL-8) (B. Fleischer, C. W. Cunningham). — For several years we have been evaluating the corrosion and erosion properties of refractory alloys in K using forced convection loop systems. A D-43 alloy loop with D-43 test section (FCL-8) was the third in a series of loops designed to evaluate the effects of boiling potassium liquid and high velocity potassium vapor on niobium-base alloys and on TZM. Operating conditions of this loop were discussed last quarter.[12] During this reporting period the loop was removed from

[12]B. Fleischer and C. W. Cunningham, Fuels and Materials Development Program Quart. Progr. Rept. June 30, 1968, ORNL-4330, pp. 85–97.

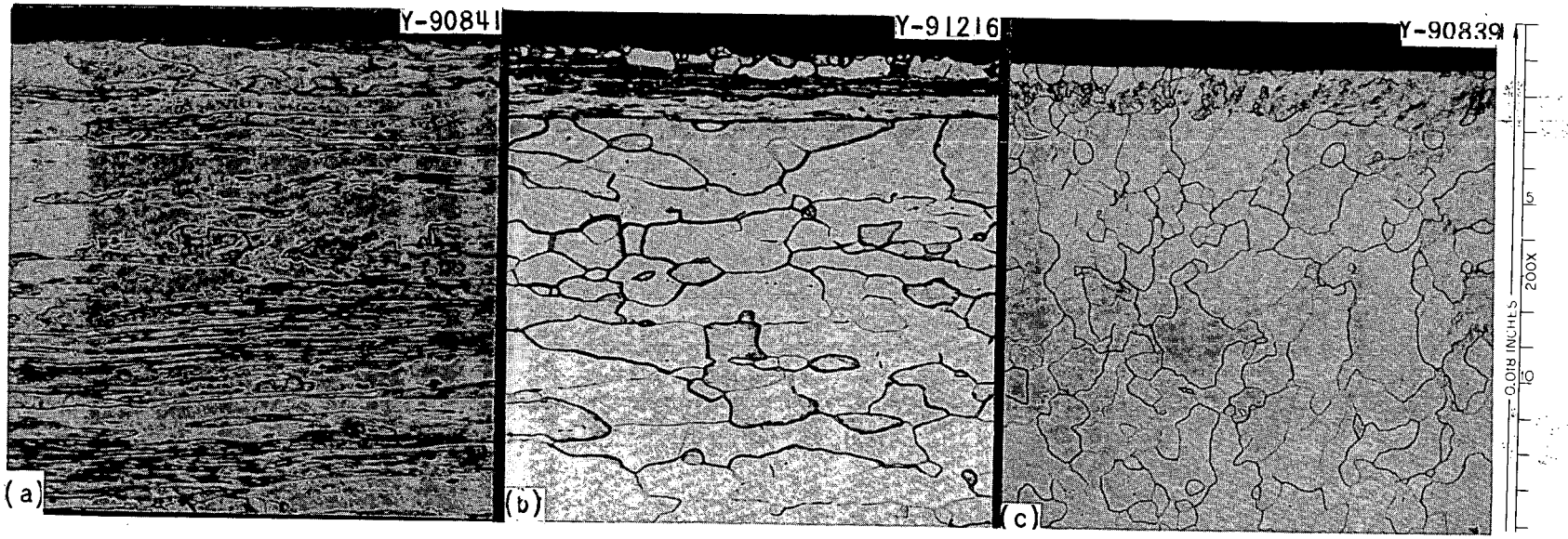

Fig. 5.16. Insert Material (a) Before Test, (b) After Test, and (c) at the Approximate Liquid-Vapor Interface. Etchant: H_2O-H_2O_2-H_2SO_4.

the vacuum chamber in which it was operated and sectioned for metallurgical examination. We are now modifying the vacuum system in preparation for the next test loop.

Liquid metal removal. The potassium inventory was drained into an evacuated tank at the end of the 10,000-hr operating period. Just before draining, the loop operating conditions were adjusted to ensure a maximum removal of the K to the dump tank:

1. The boiling conditions were adjusted to 871°C and 38.2 psia.
2. The vapor in the dryer was superheated to 996°C to supply heat to the test section.
3. The rate of heat removal to the NaK circuit was reduced to hold the condenser inlet conditions at 732°C and 12 psia.
4. The drain valve was opened to allow passage of the liquid K, driven by the combined forces of gravity and vapor pressure.
5. The potassium pump was then reversed to improve removal of liquid trapped in the helical flow passages of the pump.
6. The high temperature and the stored heat in the boiler leg, crossover line, and condenser leg dried residual pockets of K.
7. The drain valve was closed, and the loop was allowed to cool to ambient temperature to leave the loop under vacuum with only traces of condensed K.
8. The NaK economizer circuit was drained by gravity and left filled with Ar at atmospheric pressure.

We originally planned to remove any residual traces of K by distillation, but we could not do so because of a leak discovered in the NaK coolant system when the vacuum bell jar was removed. However, subsequent sectioning of the boiler and condenser revealed them to be free of K so that the distillation step was not essential.

Visual examination of boiler and condenser legs. The loop was initially sectioned into three parts as shown in Fig. 5.17. The dryer wall with its thermocouple well and heater support tabs is shown in Figs. 5.18 and 5.19. While we were trying to stabilize the loop flow, the temperature of this section reached 1370°C for a brief period. Dispite this, we saw no dimensional changes, and the only external effect noted was a general brightening of the outer surfaces.

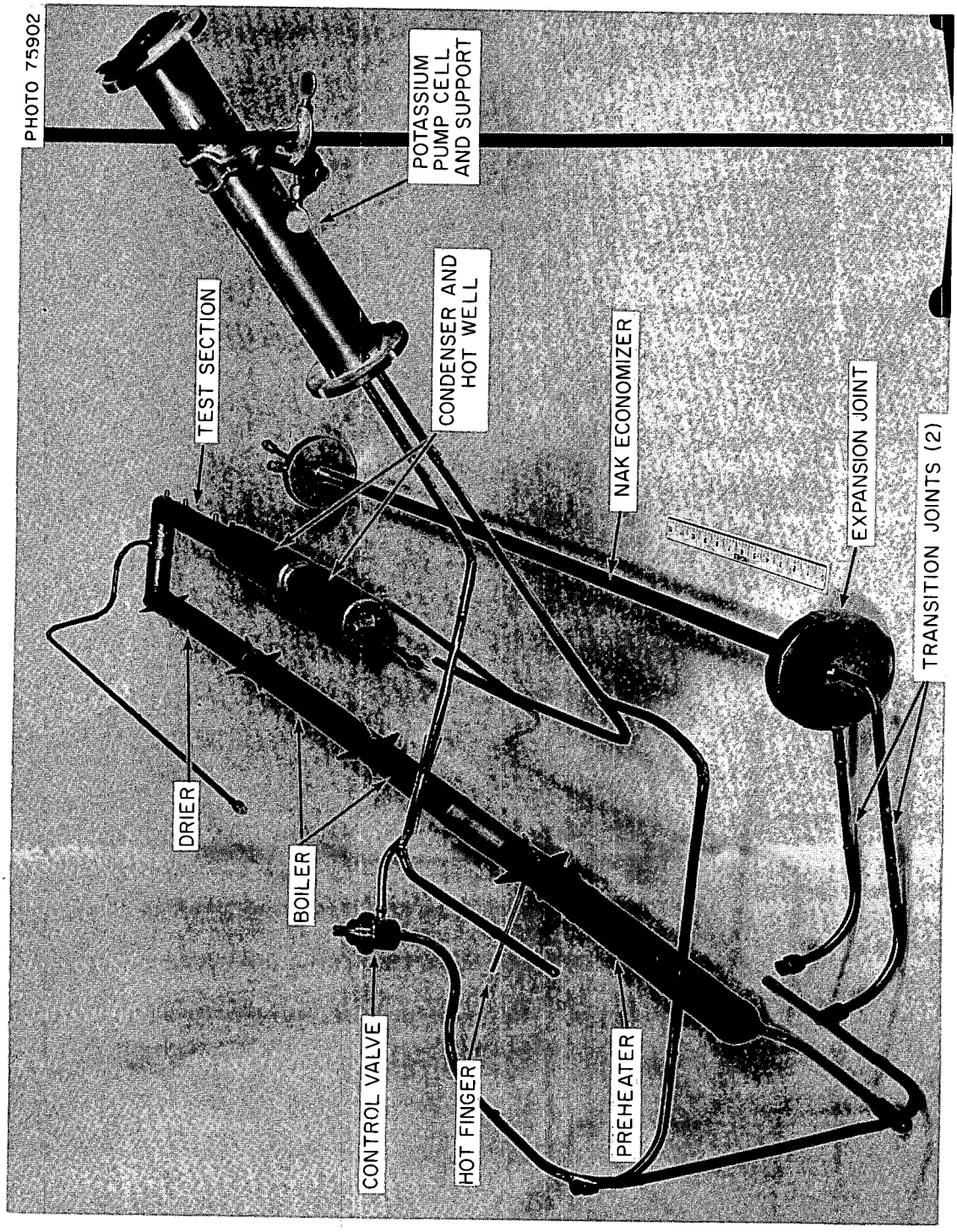

Fig. 5.17. Partially Disassembled D-43 Alloy Loop (FCL-8) After 10,000 hr of Test.

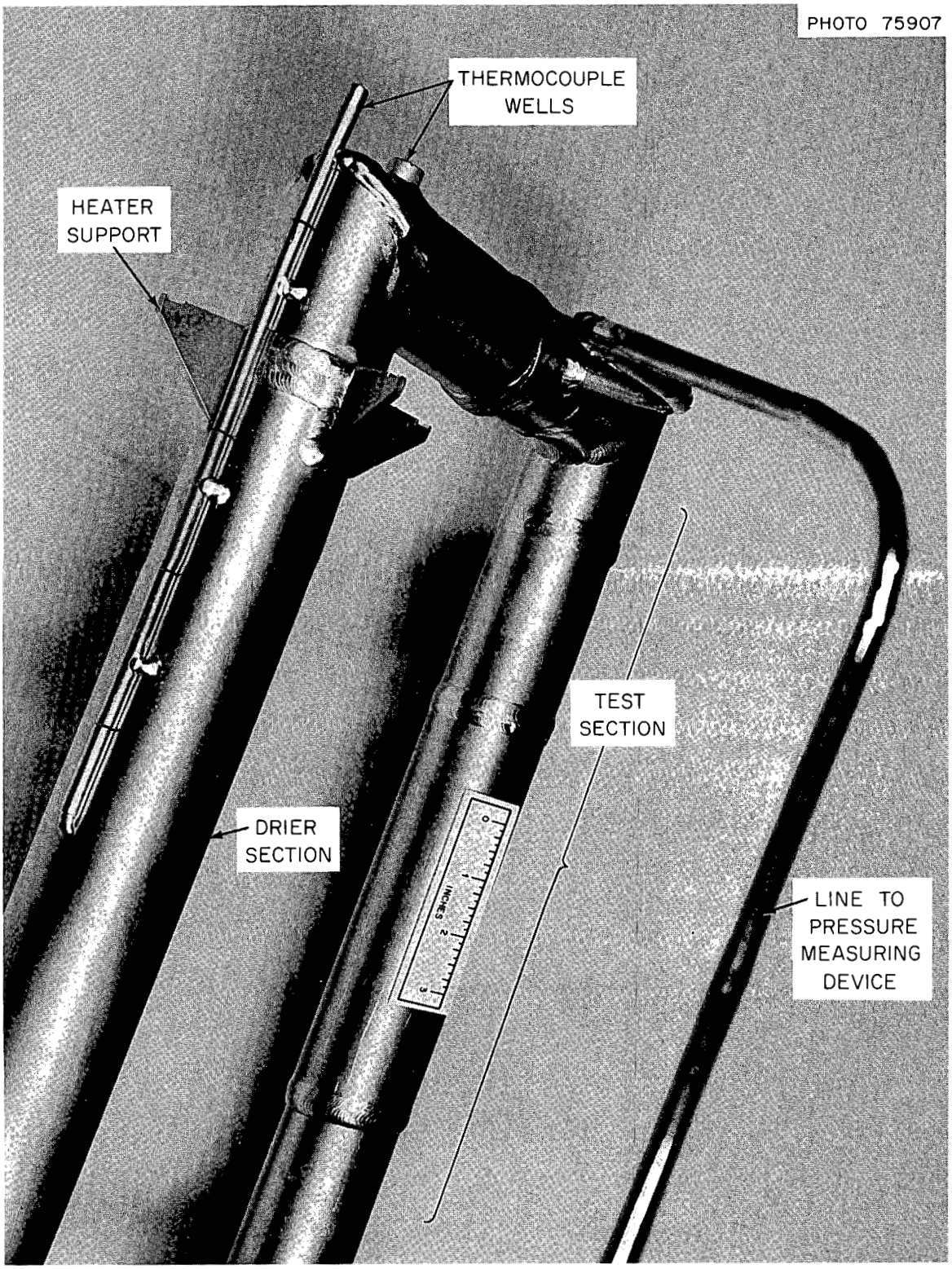

Fig. 5.18. Dryer and Test Sections of D-43 Alloy Loop (FCL-8) After Test.

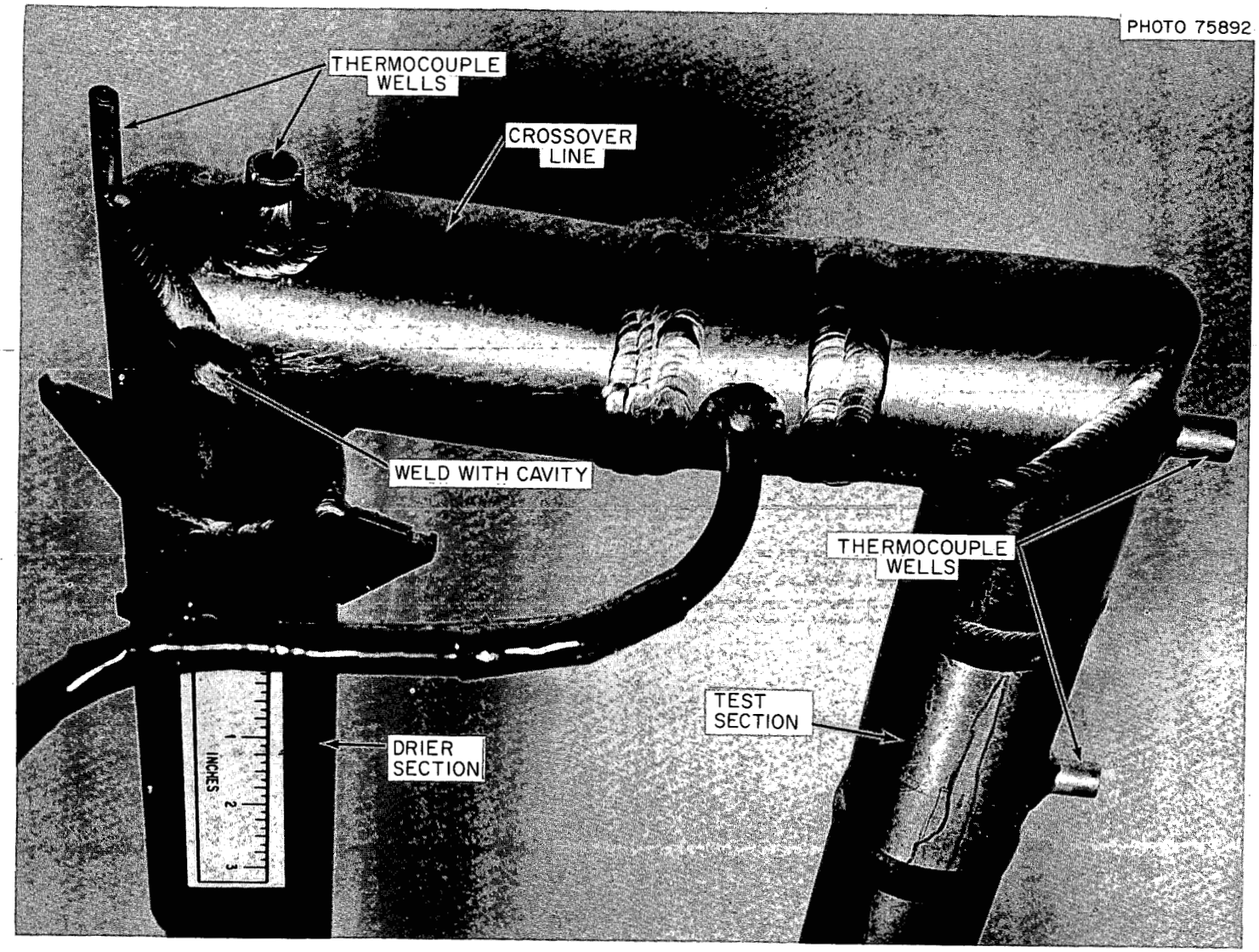

Fig. 5.19. Crossover Line Between Dryer and Test Sections of D-43 Alloy Loop (FCL-8) After Test Showing Weld Joint Complexity.

A groove apparent in one of the miter welds was made before test to eliminate a dye penetrant indication found after preoperational annealing.

Evaluation of pump. During the 10,000-hr operating period of this loop, it was necessary to increase the voltage to the potassium pump gradually to maintain a constant rate of flow in the loop. Our examination after the test disclosed decreased pump efficiency. The diameter of the exterior shell of the pump cell had increased in some areas as much as 1/32 in. X rays of the pump cell confirmed that a radial clearance of about 0.015 in. had developed between the wall and an internal helical core. The growth of the outer shell allowed bypass flows within the helical pump cell and gradually decreased the pump performance. The pressure stress on the outer shell of the pump cell would appear to have been too low to cause this extreme amount of creep. Our study of the cause of this phenomenon is still in progress.

Analysis of NaK leakage. As reported last quarter,[13] a NaK leak was detected when the vacuum chamber was opened. Visual inspection showed that the leak was very small. After we removed the protective tantalum foil wrap from the outlet line of the NaK economizer, it appeared that NaK might have leaked from the extruded Nb–1% Zr–stainless steel transition joint shown in Fig. 5.20. Dye penetrant inspection of this piece revealed a small defect on the outer surface at the interface between the Nb–1% Zr and stainless steel. X-ray inspection also showed a delamination type of defect on the interior surface. The joint was removed from the piping system, thoroughly washed in alcohol and boiling water, and then checked for leakage on a helium leak detector. No leak was indicated, but we cut the joint longitudinally and found that the interior surface was indeed delaminated at several areas where the Nb–1% Zr tapered into the stainless steel. Hence we would conclude that the leakage of NaK occurred because of this defective area in the transition joint. The rate of leakage was probably quite small, and therefore it is conceivable that NaK had been leaking into the vacuum vessel long before the end of the test.

---

[13]B. Fleischer and C. W. Cunningham, Fuels and Materials Development Program Quart. Progr. Rept. June 30, 1968, ORNL-4330, pp. 85–97.

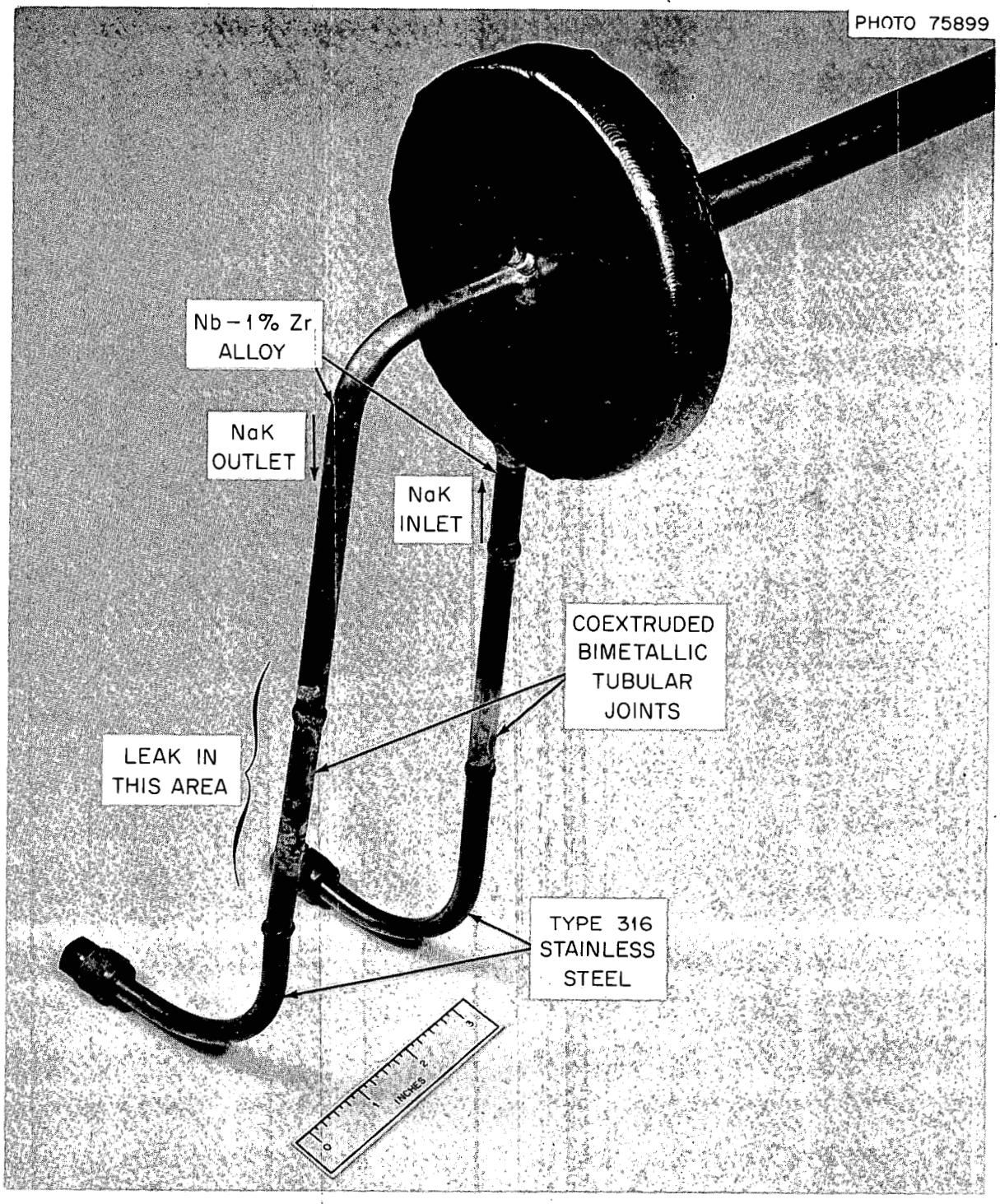

Fig. 5.20. Region of Small NaK Leak in D-43 Alloy Loop (FCL-8). Leak due to metal delamination in extruded Nb–1% Zr–stainless steel transition joint from economizer.

Inspection of vacuum chamber. During the test, we found an air leak in the area where the ion pump wells were welded to the vacuum chamber wall. However, the ion pumping capacity was sufficient to hold the chamber in the low (10^{-8} torr) range. A dye penetrant examination after test revealed a defect extending completely across this weld. A second defect was found in another weld. Both welds are being repaired and strengthened by overlaying weld metal around the entire joint. The nitrogen component observed in the residual gas during loop operation can be explained by this leak. The oxygen component was missing; we believe it was effectively consumed by the leaking NaK. The argon component can be explained in part by the air leak and in part by a possible leak from an argon-filled thermocouple assembly.

Refurbishing of triode ion pumps. The triode ion pumps were reconditioned at the vendor's plant, where the cathode construction was changed. The titanium wire and the supporting stainless steel of the cathode were replaced by an all-titanium expanded-metal-screen cathode construction. The vendor has found that the elimination of sputterable stainless steel is advantageous.

Interim vacuum test. Preparations are being made for a vacuum test before installing the next test loop into the chamber. This test will serve to verify the leak-tightness of the chamber, to determine the performance of the reconditioned ion pumps, and to evaluate the integrity of both new and old penetrations that are required for the next test.

Posttest examination. The main loop was sectioned as shown in the diagram in Fig. 5.21. Each section was cleaned with butyl, methyl, and ethyl alcohols to ensure safe removal of all unreacted K. No residual potassium metal was found during this cleaning. All parts were then rinsed 30 min with hot flowing water, dried with an alcohol rinse, and capped to await further examination.

All auxiliary piping lines were examined for residual K. Any K found was removed by melting under kerosene. These lines and the pump cell, valve, and economizer were then cleaned as previously described for the main loop.

Visual inspection of all pieces before and after cleaning showed no evidence of mass transfer. When the test pieces were removed, a

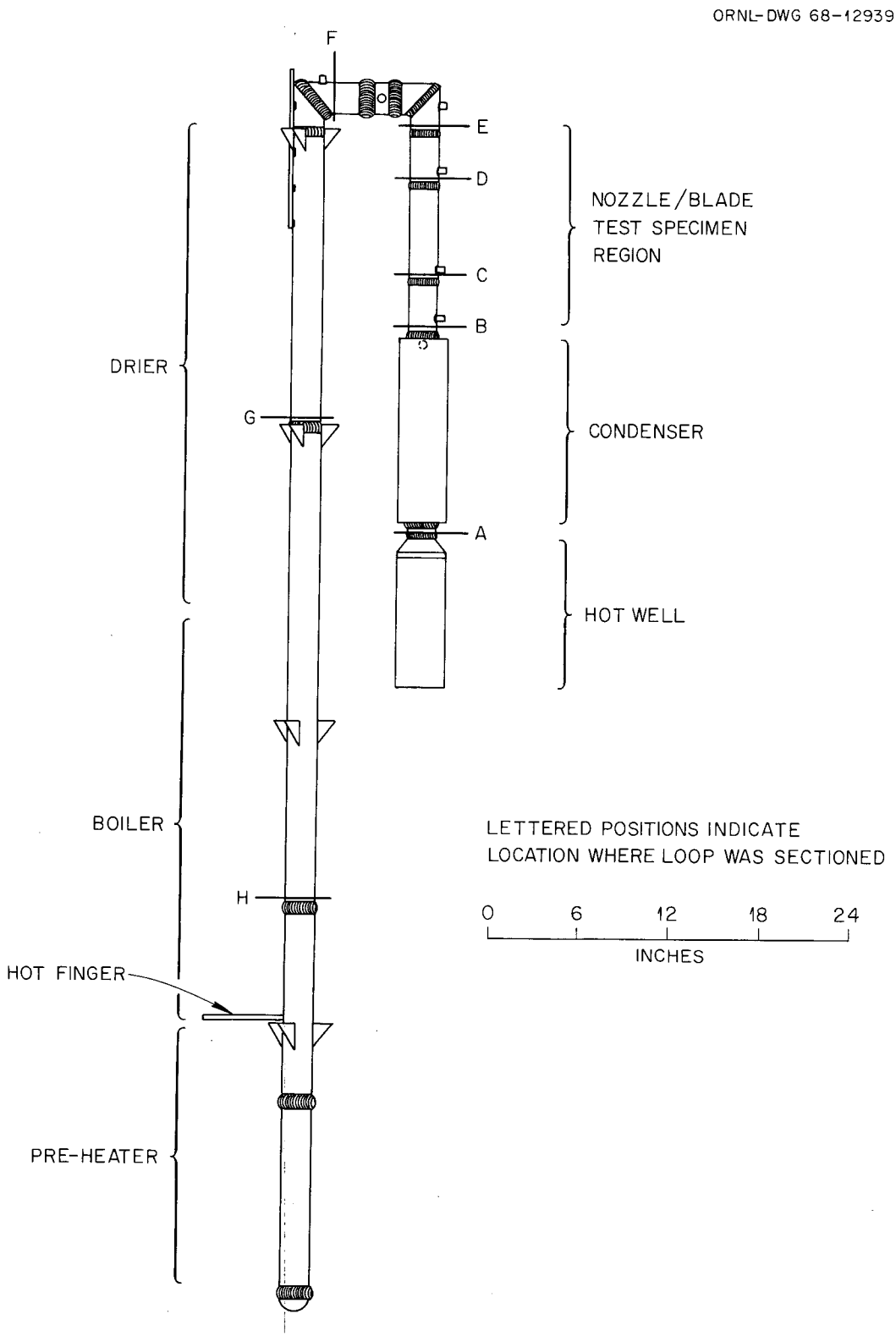

Fig. 5.21. Sketch of D-43 Alloy Loop (FCL-8) Showing Loop Sectioning Plan for Posttest Inspection.

small discolored area was noted on blade 2 at the vapor stream impingement point.

Effect of Oxygen on Compatibility of Refractory Metals and Alkali Metals (R. L. Klueh)

Oxygen Effects in the Tantalum-Potassium System. — We have completed our evaluation of the Ta-O-K system at 800 and 1000°C (ref. 14). The studies supplement those completed earlier on the Nb-O-K system.[15] In addition to providing data on equilibrium states, the tests were designed to yield data on the kinetics of weight changes of the tantalum specimens resulting from oxygen diffusion and tantalum dissolution. However, because of the rapid dissolution and because the specimens in some cases were penetrated by the K, the kinetics data are, at best, qualitative.

Table 5.4 shows the temperature, time, and oxygen conditions investigated in this test series. Potassium penetrated all but one of the tantalum specimens to which O had been added before testing (i.e., specimens containing $\geq$ 650 ppm O). Figures 5.22, 5.23, and 5.24 show the appearance of tantalum specimens containing 680, 1200, and 1800 ppm O after exposure to K at 800°C; each of the specimens exhibits attack preferentially along grain boundaries. Figure 5.24 is especially interesting because of the unusual grain structure of the Ta (i.e., the elongated grains parallel to the "flat" edge of the specimen). Compare the relatively deep penetration in the longitudinal direction with the shallower penetration in the transverse direction. Attack in the latter direction was confined to a band of small, equiaxed grains near the surface and was halted by grains elongated in the direction of rolling — confirmation that only grain-boundary attack is occurring. We believe that attack proceeds with the formation of a ternary oxide which then dissolves in K as the system tends toward equilibrium. This, as well as loss during metallographic preparation, could explain the apparent absence of corrosion products in the after-test microstructures.

---

[14]R. L. Klueh, Fuels and Materials Development Program Quart. Progr. Rept. June 30, 1968, ORNL-4330, pp. 142–146.

[15]A. P. Litman, The Effect of Oxygen on the Corrosion of Niobium by Liquid Potassium, ORNL-3751 (July 1965).

Table 5.4. Effect of Oxygen on Compatibility of Tantalum and Potassium

Temperature (°C)	Time (hr)	Oxygen in Potassium (ppm)	Oxygen in Tantalum (ppm)		Weight Change (mg/cm^2)	Tantalum in Potassium (ppm)
		Before	Before	After		After
800	1	1900	50	43	−0.0585	1890
	3	2000	50	29	−0.0594	2990
	5	1880	50	26	−0.0741	3200
	100	2000	50	19	−0.1520	2640
	100	490	680	34	−1.950	2480
	100	1970	650	36	−1.880	3120
	100	1950	1200	36	−3.240	7570
	100	1980	1800	32	−6.650	6850
1000	0.5	2020	50	39	−0.0460	3860
	1	1930	50	38	−0.0645	3830
	2	2020	50	50	−0.0745	4620
	50	2010	50	48	−0.202	14,120
	0.5	100	1600	120	−5.91	3680
	1	100	1600	210	−5.86	4980
	2	100	1600	36	−6.06	5110
	50	100	1700	23	−6.28	6830
	50	450	620	39	−1.92	9640
	50	1980	660	43	−1.86	15,070
	50	1970	1000	53	−3.23	7780
	50	1930	1900	53	−6.50	20,600

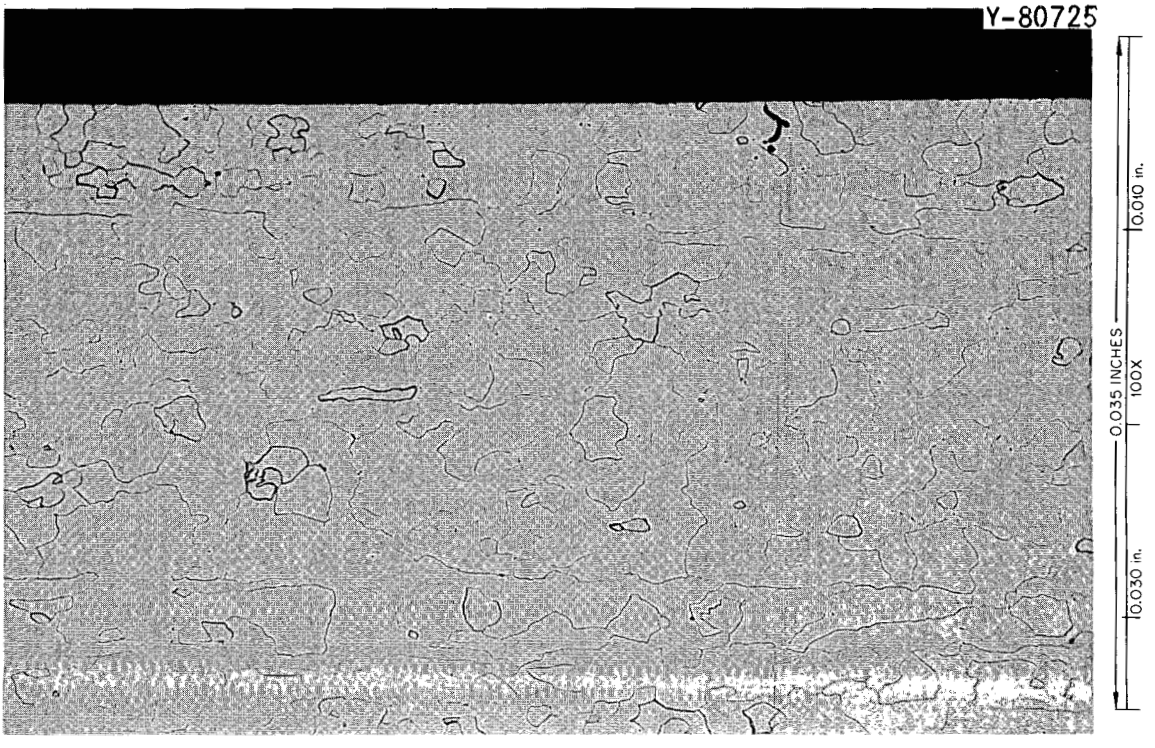

Fig. 5.22. Tantalum, Which Initially Contained 680 ppm O, After Exposure to Potassium for 100 hr at 800°C. Etched in a solution of H_2O, HNO_3, and NH_4HF.

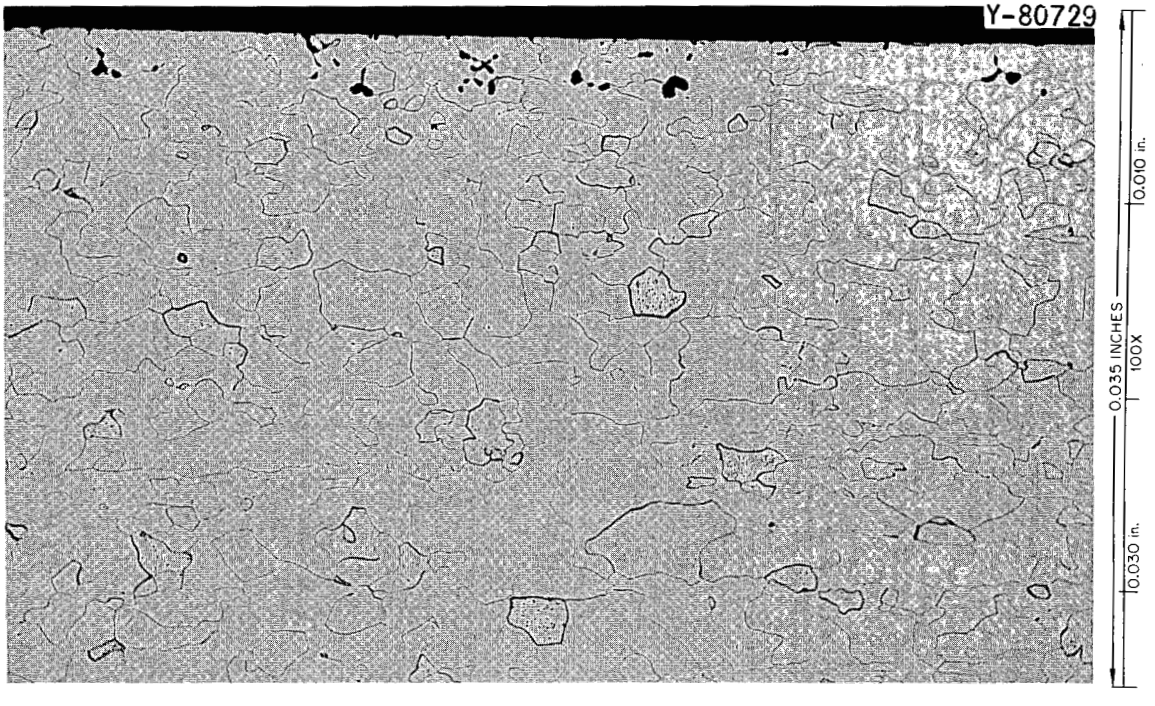

Fig. 5.23. Tantalum, Which Initially Contained 1200 ppm O, After Exposure to Potassium for 100 hr at 800°C. Etched in a solution of H_2O, HNO_3, and NH_4HF.

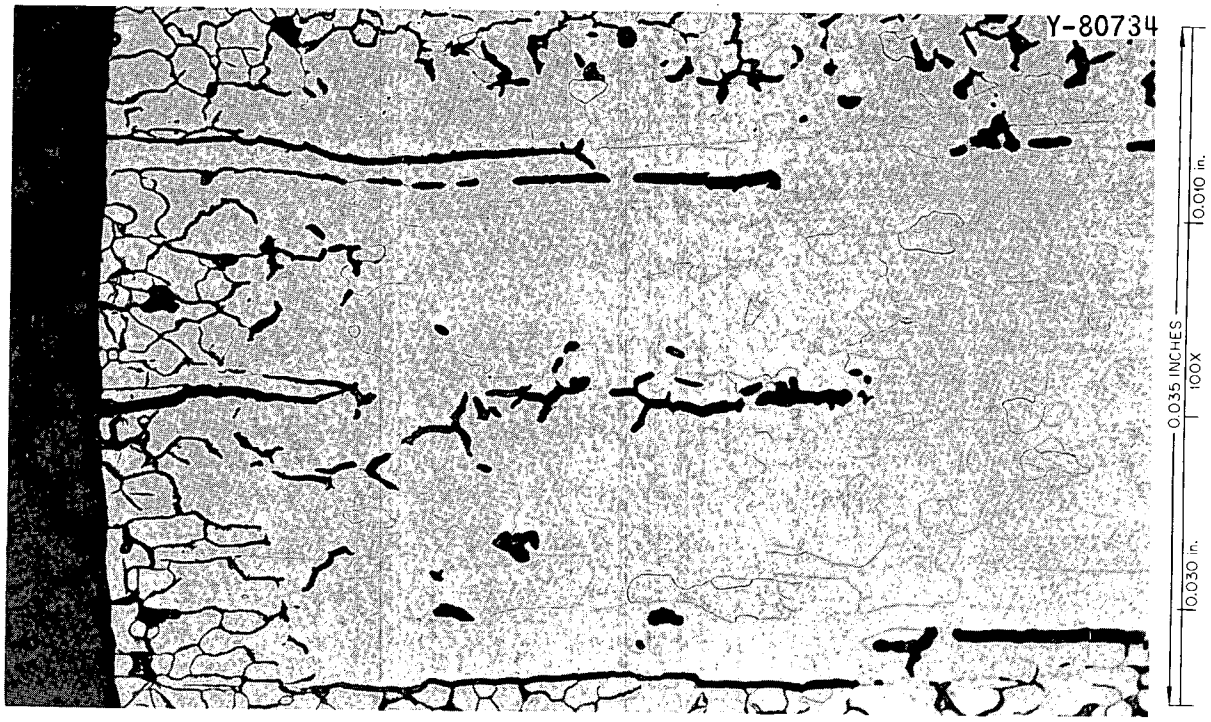

Fig. 5.24. Tantalum, Which Initially Contained 1800 ppm O, After Exposure to Potassium for 100 hr at 800°C. Etched in a solution of H_2O, HNO_3, and NH_4HF.

At 1000°C, the addition of 660 ppm O to Ta did not affect attack by K, and little attack (similar to Fig. 5.22 at 800°C) was noted for the specimen containing 1000 ppm O. Heavy attack at 1000°C resulted for a tantalum specimen containing 1600 ppm O after 1 hr exposure to K, as shown in Fig. 5.25.

These results are qualitatively similar to those obtained by DiStefano[16] for the Nb-O-Li and Ta-O-Li systems: (1) a threshold concentration of O in the Ta must be exceeded before penetration occurs (this level increases with increasing exposure temperature); (2) above this threshold level, the amount of attack (i.e., depth of penetration) increases with an increase in the initial concentration of O in the Ta; (3) the attack is not affected by the concentration of O in the K; (4) when O_2 diffuses out of the specimen rapidly, as at 1000°C, it

[16]J. R. DiStefano, Corrosion of Refractory Metals by Lithium, ORNL-3551 (April 1966).

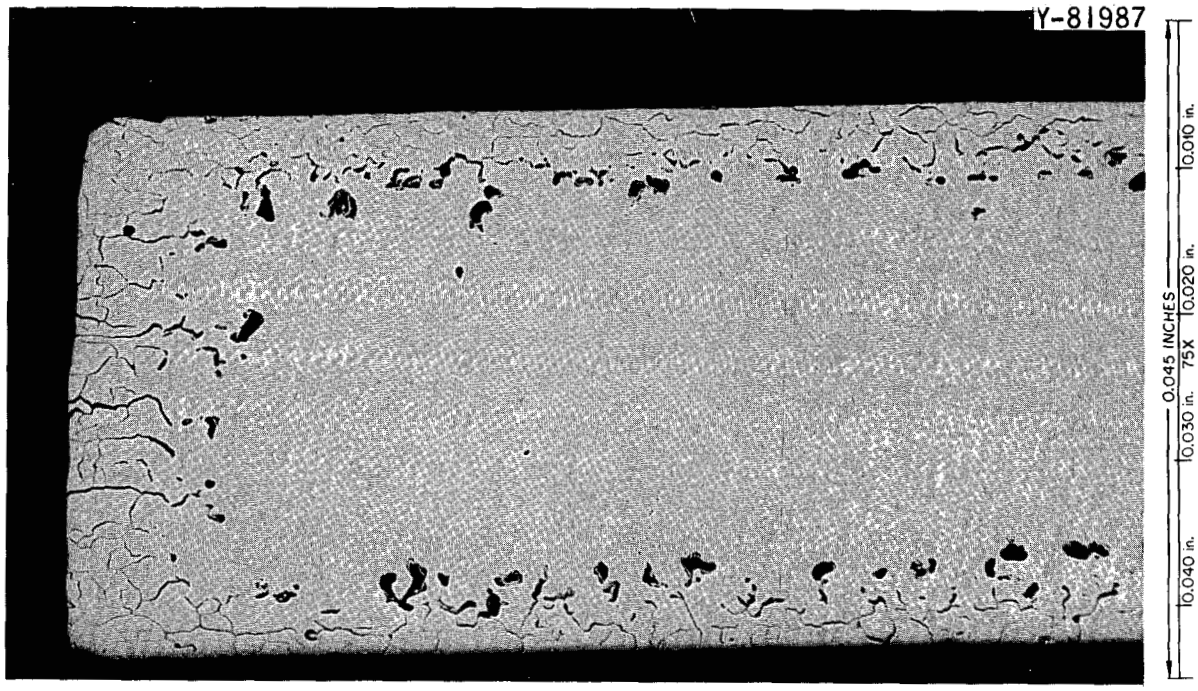

Fig. 5.25. Tantalum, Which Initially Contained 1600 ppm O, After Exposure to Potassium for 0.5 hr at 1000°C. As polished.

limits the depth of penetration. The chief difference between the present studies and DiStefano's studies of Li is that the latter showed attack to occur in Ta at 815°C with as little as 300 ppm O (ref. 16). This would indicate that the threshold concentration is higher for penetration by K than by Li.

As shown in Table 5.4, the concentration of Ta in the K increased as the level of O in the K increased. (The final concentration of O in the K is somewhat larger than that shown in Table 5.4 because of O donated by the Ta of the container and specimen.) Since we believe penetration involves the formation of a compound containing O, the final concentration of O in the penetrated specimens may include O in the form of a corrosion product as well as O dissolved in the Ta.

The specimens exposed to K with a high concentration of O contained a dark scale. When we tried to identify the scale by x-ray diffraction, we detected only tantalum metal. Furthermore, within experimental error, removal of the scale from the specimen did not change the oxygen content of the specimen.

Oxygen Effects in the Niobium-Sodium System. — The results of the Ta-O-K system discussed above, together with previous studies[16,17] at ORNL, indicate that there is a marked difference in the effect of O on the compatibility of refractory metals and alkali metals depending upon whether O is present in the refractory metal or the alkali metal. We are attempting to categorize these different effects in the Nb-O-K, Ta-O-K, Nb-O-Na, Ta-O-Na, Nb-O-Li, and Ta-O-Li systems. For these studies we are using static capsules of the configuration previously described for studies of Ta-O-K (ref. 18). All tests are being conducted at 600°C, since this temperature is of direct interest in sodium-cooled fast breeder reactor applications.

Our first tests in this series were conducted on the Nb-O-Na system. Four capsules containing unoxidized niobium specimens were exposed to Na with several oxygen levels, and two capsules containing niobium specimens with 950 and 1600 ppm O, respectively, were exposed to Na with about 50 ppm O.

All tests were conducted for 500 hr. Results are shown in Table 5.5. Although the specimens appeared dull after test, none of them appeared to have a scale. All specimens showed weight losses. The two oxidized specimens showed considerable oxygen loss, while the unoxidized specimens showed little oxygen change. Diffusion calculations and microhardness profiles of the unpenetrated specimens indicated that the oxygen concentration was near equilibrium after 500 hr at 600°C.

Metallographic examination of the two oxidized specimens indicated that they had been penetrated by the Na. The penetration was much less severe than for similarly oxidized tantalum specimens exposed to K at 600°C (ref. 19). As in the case of these Ta-O-K tests, the final oxygen concentration in the Nb-O-Na tests may include O present as an internal corrosion product as well as O in solid solution.

---

[17]A. P. Litman, The Effect of Oxygen on the Corrosion of Niobium by Liquid Potassium, ORNL-3751 (July 1965).

[18]R. L. Klueh, Fuels and Materials Development Program Quart. Progr. Rept. June 30, 1968, ORNL-4330, p. 142.

[19]R. L. Klueh, "Oxygen Effects in the Tantalum-Potassium System," pp. 120–124, this report.

Table 5.5. Effect of Oxygen on Compatibility of Niobium and Sodium at 600°C

Oxygen in Sodium[a] (ppm) Before	Oxygen in Niobium (ppm) Before[b]	Oxygen in Niobium (ppm) After[b]	Weight Change[c] (mg)	Niobium in Sodium (ppm) After
50	70	59	−0.1	400
300	70	62	−0.5	800
700	70	64	−2.0	1400
1000	70	83	−1.7	2200
50	950	540[d]	−1.7	500
50	1600	440[d]	−6.2	1000

[a]Oxygen added as Na_2O to Na containing about 50 ppm O.

[b]Determined by vacuum-fusion analysis.

[c]All specimens were 1 × 0.5 × 0.04 in.

[d]Microstructures show that Na penetrated these specimens.

Partitioning of Oxygen Between Potassium and Zirconium and Sodium and Zirconium. — As noted in the previous report[20] we have re-examined the value originally assigned to the equilibrium distribution coefficient for the distribution of O between Zr and K (i.e., $\kappa^O = \frac{\text{atom fraction of O in Zr}}{\text{atom fraction of O in K}}$). Below we will demonstrate why we believe that the equilibrium distribution coefficient at 815°C is much larger than originally thought and then show how this new coefficient affects the gettering-vacuum-fusion (GVF) method for determining oxygen concentrations in K (and Na).

Zirconium containing 1 wt % O, when exposed at 815°C to triple-gettered K (< 10 ppm O), gained a small amount of weight and increased in O (ref. 21). This result can be used to set limits on the distribution coefficient, κ^O, at 815°C. Taking 10 ppm O as the upper limit for

[20]R. L. Klueh, Fuels and Materials Development Program Quart. Progr. Rept. June 30, 1968, ORNL-4330, p. 146.

[21]A. P. Litman, private communication.

the after-test concentration of O in the K, it follows that $\kappa^{O}_{815°C} > 2 \times 10^{3}$. But since the concentration was probably closer to 1 ppm O after test, $\kappa^{O}_{815°C}$ more reasonably approaches 10^{4} or higher.

Using the oxidation data of Mackay[22] for Zr in Na along with recent solubility data for O in Na (ref. 23) and following the same argument as above, we find that κ^{O} for Na at 635°C must be greater than 5×10^{4}. This is in accord with Mackay's results, which showed that Zr could be oxidized at 635°C in Na that had an oxygen concentration determined by a cold trap operating at 160°C. Theoretical calculations of κ^{O} suggest that the coefficient should not change by more than an order of magnitude at 800°C, the temperature of the GVF anneal.

Once κ^{O} has been established as being very much larger than unity, it follows, under the conditions of our GVF analysis technique, that when pure Zr is exposed to K or Na containing O, essentially all of the O is gettered by the Zr. Therefore, the amount of O originally present in the liquid, $C_{O}^{(A)}$, is given by

$$C_{O}^{(A)} = \Delta C_{O}^{(Zr)} \frac{W_{Zr}}{W_{A}} \quad , \tag{5.1}$$

where $\Delta C_{O}^{(Zr)}$ is the O gettered by the Zr and W_{Zr} and W_{A} are the weights of the Zr and alkali metal, respectively. The distribution coefficient, being effectively infinite, does not enter into the calculation.

We are now conducting recovery tests designed to verify Eq. (5.1).

Corrosion of Refractory Alloys by Lithium

Thermal Convection Loop Tests (J. H. DeVan). — The sixth in a series of lithium thermal convection loop tests designed to study mass transfer of refractory metals was terminated after completing a 3000-hr test run. This loop, TCL-6R, was fabricated of the tantalum-base alloy T-222 and operated at a maximum hot-leg temperature of 1350°C. Compositions of the

---

[21] T. L. Mackay, Oxidation of Zirconium and Zirconium Alloys in Liquid Sodium, NAA-SR-6674 (February 1962).

[22] V. J. Rutkauskas, Determination of the Solubility of Oxygen in Sodium by Vacuum Distillation, LA-3879, Los Alamos Scientific Laboratory (September 17, 1968).

loop tubing and insert specimens are given in Table 5.6, and flow rate and temperature conditions for the test are shown below:

Maximum hot-leg temperature, °C	1350
Minimum cold-leg temperature, °C	1140
Lithium flow rate, g/min	240
Lithium velocity, cm/sec	2.5
Test duration, hr	3000

After operation, the loop was drained to collect a sample of Li and was then flushed with liquid ammonia to remove residual Li. Eighty-two sheet specimens were then removed and tested for weight change, chemistry, and metallographic condition.

The weight-change results are shown in Fig. 5.26. The weight change around the loop was analogous to that observed for Nb–1% Zr and D-43 at 1200°C, where about two-thirds of the loop surface lost weight and one-third gained weight. Also, as in the niobium alloy loops, specimens from the weight gain region of this loop were covered by a thin, gold-colored film. As would be expected from the small magnitude of the weight changes for the T-222 specimens, no dimensional changes could be detected on any of the specimens.

Chemical analyses of the insert specimens, although not complete, have shown a significant transport of Hf from the hotter to the cooler loop surfaces. X-ray fluorescence was used to evaluate the concentration of Hf near the surface of the insert specimens; the results are shown in Fig. 5.27. Note that the profile of the hafnium surface concentration around the loop mirrors the weight-change profile shown in Fig. 5.26:

Table 5.6. Compositions of T-222 Components Used in Loop TCL-6R

Loop Component[a]	Chemical Composition, wt %					
	W	Hf	O	N	C	Ta
Insert Specimens (0.030 × 1 × 0.8 in.)	10.2	2.3	0.005	0.004	0.014	Bal
Loop Tubing (1 in. outside diameter × 0.065 in. wall thickness)	10.3	2.2	0.003	0.002	0.013	Bal

[a]Loop annealed after assembly for 2 hr at 1300°C.

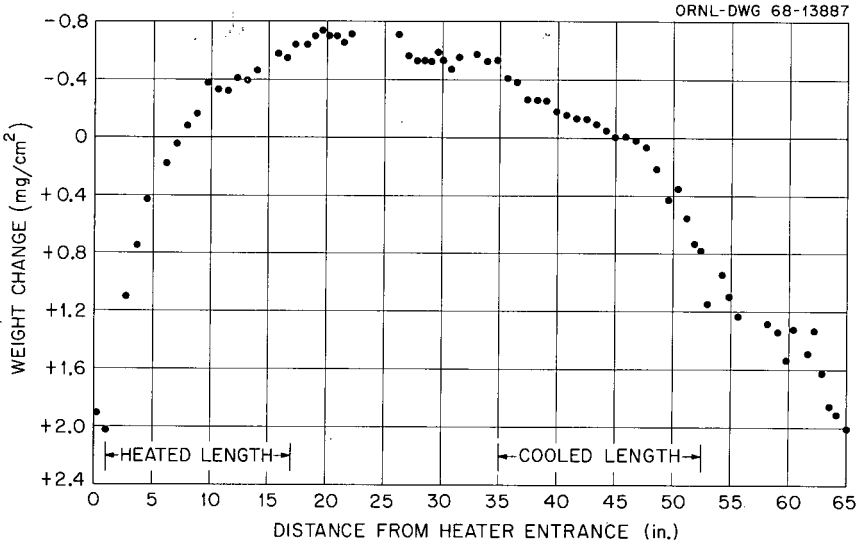

Fig. 5.26. Weight Change of T-222 Thermal Convection Loop After Operating with Lithium for 3000 hr at 1350°C.

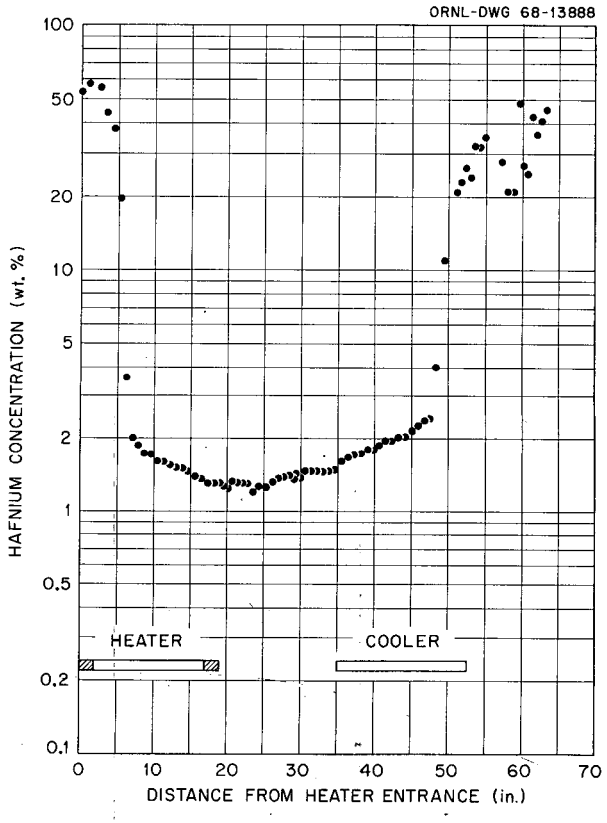

Fig. 5.27. Hafnium Concentration Near Surfaces of T-222 Insert Specimen After Operation with Lithium. Analyzed by x-ray fluorescence.

regions of weight loss reflect hafnium depletion while regions of weight gain reflect hafnium enrichment.

Additional metallographic and chemical analyses of loop sections and insert specimens are in progress.

T-111 Forced Circulation Loop (FCLLL-1). – Loop equipment and design. (D. L. Clark) All design work has been completed, and drawings have been issued for construction. Work has continued on the T-111 alloy test-bed loop for studying new refractory alloys at very high temperatures in high-velocity liquid Li. Installation of component parts and assemblies is being delayed until completion of the preliminary check-out of the reworked triode ion pumps. All available vacuum penetrations are being installed for check-out during this period. Included will be the 3000-amp electrical feedthrough, the flange penetration for the fill and drain, and sampling systems, the part for the optical pyrometer, and the can and flange for the helical induction pump.

Fabrication of T-111 assemblies. (B. Fleischer) We completed welding of the radiator, heater section, economizer, and pump lines. We fabricated the radiator coil by butt welding straight pieces of tubing together and then bending them. All welds were inspected after bending and found to be free of cracks. The ends of the coil were then cut off and prepared as subassemblies to facilitate welding of thermocouple wells, end caps, and inlet and outlet tubing. The subassemblies were then butt welded to the main coil.

The economizer, heater section, and pump lines were constructed by welding of component parts previously bent and machined in accordance with detail drawings. We experienced considerable difficulty in attempting to achieve dimensional tolerances and proper alignment. To check for proper mating of the economizer, radiator, and heater sections, we placed the parts on the test stand and aligned them with respect to the copper bus assembly. Additional bending of portions of the economizer and heater sections was required to properly mate the parts.

Annealing of T-111 welds. (B. Fleischer) Welds of T-111 severely contaminated with O will fail rapidly when exposed to Li. This problem can be alleviated by annealing the welds for several hours at 1315°C before exposing them to Li. Even though the welds we made in assembling

FCLLL-1 were performed under clean, inert conditions in a dry box, the possibility of undiscovered weld contamination made it prudent to anneal. The cost of this insurance is inconsequential compared to the cost of materials and labor already invested in the assemblies.

Accordingly, we prepared the assemblies for annealing by an outside contractor. The loop surfaces were wiped with lint-free cloths soaked in alcohol and then wrapped spirally at about 3/4-in. pitch with 0.060-in.-diam tantalum wire. Tantalum foil 0.001-in. thick by 2-in. wide was wrapped at half lap over the wire, which serves as a spacer to prevent welding of the foil to the parts. The foil acts as a mechanical barrier to minimize environmental contamination.

We annealed these subassemblies in a 12-ft-long by 4-ft-diam vacuum furnace located in the Refractory Metal Center, Materials Systems Division, Union Carbide Corporation, Kokomo, Indiana. The annealing cycle is described in Table 5.7. The temperature of the parts was determined by placing Pt–6% Rh vs Pt–30% Rh thermocouples at anticipated heat-lag locations. Sample coupons of T-111 were placed at various locations to check contamination.

After annealing, all the foil and parts were still bright. An unwrapped T-111 control specimen was bent 90° without any evidence of cracking. Analysis of the control specimens reported in Table 5.8 showed no contamination of wrapped or unwrapped specimens.

Fabrication of control specimen units. (D. L. Clark, B. Fleischer) Furnaces for the exposing of control specimens have been fabricated. The units are shown in Fig. 5.28. Figure 5.29 shows the control specimen material mounted on the holders. One of the furnaces will be used to expose the specimens at 1370°C while the other will operate at 1205°C. The units will be mounted on the top of the test stand. These specimens will be used for comparison of mechanical properties of the same material exposed at the same temperature to Li inside the loop.

Table 5.7. Vacuum Annealing Cycle for FCLLL-1 T-111 Loop

Time (pm)	Description of Operation	Temperature, °C			Vacuum Pressure (torr)
		Furnace	Parts[a]		
			Position 1	Position 2	
					$\times 10^{-7}$
12:30	Start heatup				200.0
1:00	Start 260°C hold	260			270.0
1:25	End 260°C hold	260			80.0
1:35		315			290.0
2:10	Start 540°C hold	540	305	345	120.0
2:35	End 540°C hold	540	420	445	44.0
3:00		705			330.0
3:15	Start 815°C hold	815	670	705	170.0
3:30	End 815°C hold	815	760	780	73.0
3:40	Realign vacuum instruments	870			90.0
		870			190.0
4:05	Start 1095°C hold	1095	1010	1030	320.0
4:20	End 1095°C hold	1095	1060	1070	210.0
4:35		1315	1250	1270	650.0
4:45	Start 2-hr anneal	1330	1290	1300	540.0
5:05		1330	1310	1315	230.0
6:45	End 2-hr anneal (start controlled cool down)	1330	1310	1315	63.0
7:20	Cut off all furnace power	815	860	860	7.5
7:35		540			5.6
8:35		260			5
11:55		95			6.7

[a]Thermocouples placed arbitrarily at anticipated heat-lag positions.

Table 5.8. Interstitial Element Concentration of Control Samples During FCLLL-1 Anneal

Specimen Description	Concentration, ppm							
	Unwrapped				Wrapped[a]			
	C	O	N	H	C	O	N	H
Unexposed control specimen	90	140	12	3	70	140	7	4
Exposed at top of furnace	80	150	7	12	70	140	8	1
Exposed at bottom of furnace	70	140	10	7	70	140	13	1

[a]These specimens were wrapped with two layers of 0.001-in.-thick tantalum foil.

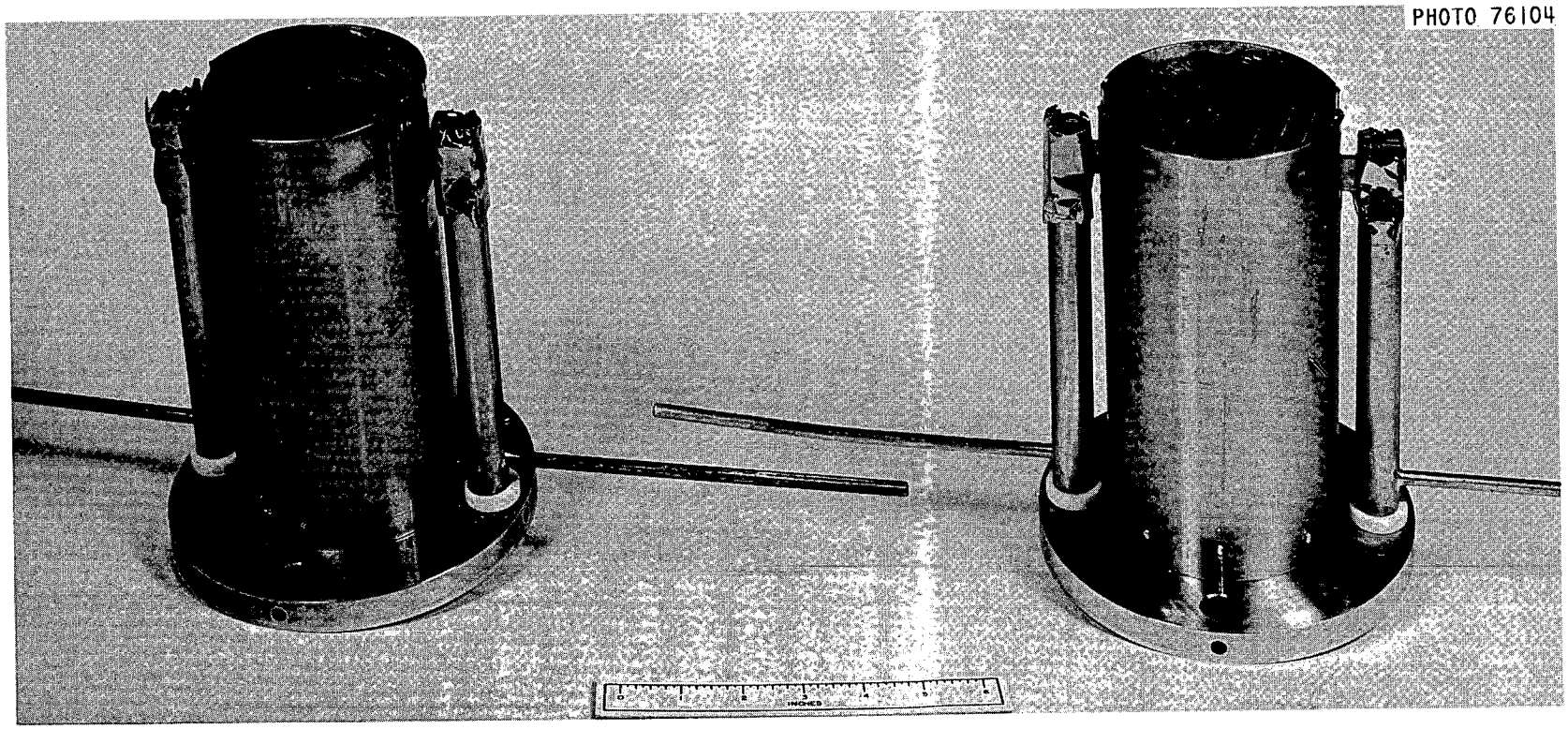

Fig. 5.28. Furnaces for FCLLL-1 Control Specimens.

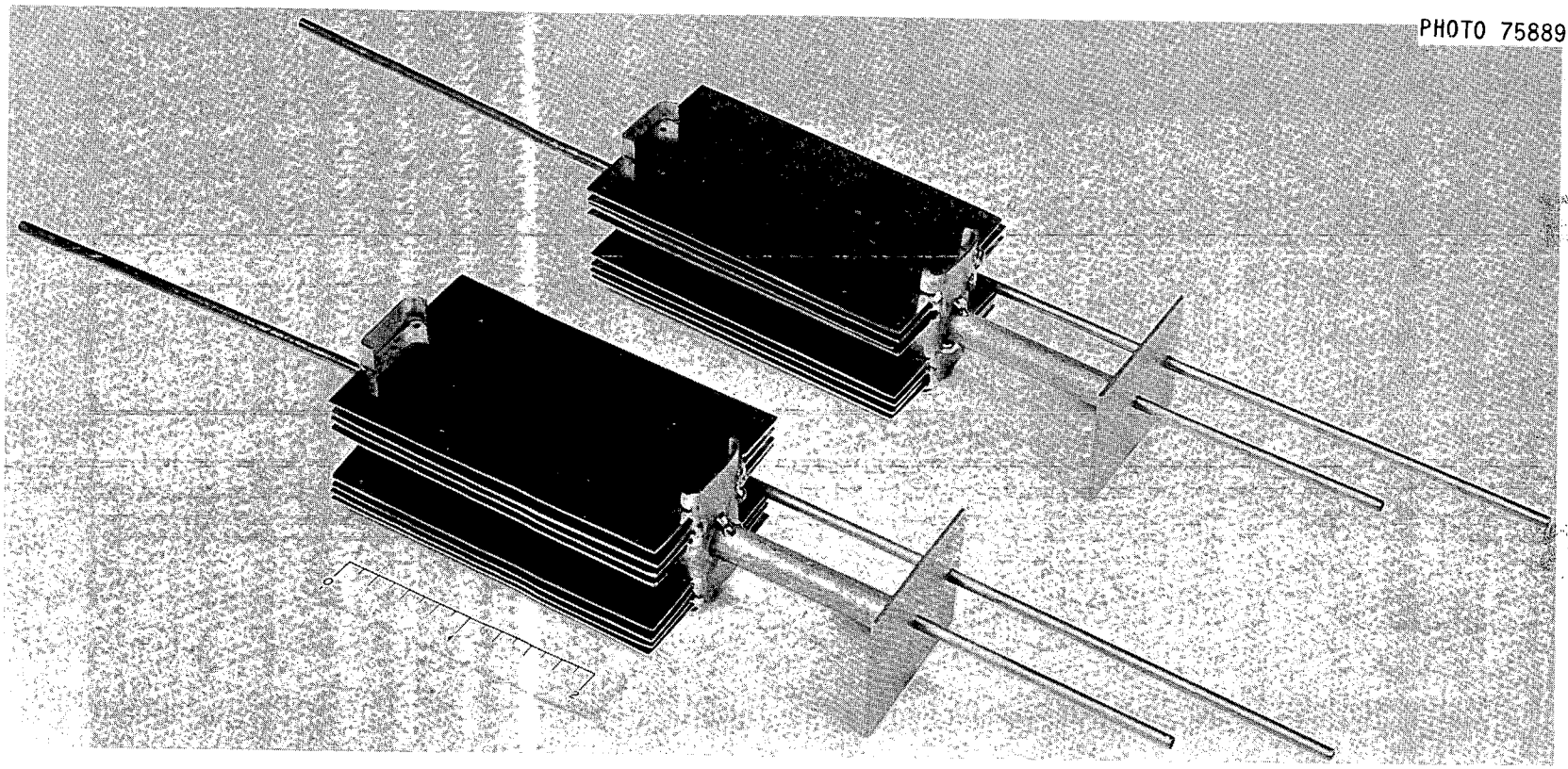

Fig. 5.29. Control Specimens of T-111 Alloy for FCLLL-1.